Univerzita Tomáše Bati ve Zlíně
Fakulta technologická

Doctoral Thesis

Struktura a lomové chování pryže

Structure and fracture behaviour of rubber

Autor: **Ing. Ondřej Kratina**

Studijní program: Chemie a technologie materiálů
Studijní obor: Technologie makromolekulárních látek

Školitel: doc. Ing. Roman Čermák, Ph.D.

Konzultanti: Dr.-Ing. Radek Stoček
Ing. Martina Polášková, Ph.D.

Zlín, říjen 2017

© Ondřej Kratina

Vydala **Univerzita Tomáše Bati ve Zlíně** v edici **Doctoral Thesis.**
Publikace byla vydána v roce 2017

Klíčová slova: *pryž, kaučuková směs, lomová mechanika, trhlina, iniciace, šíření, lom, únava, oděr, mechanické zatížení*

Key words: *rubber, rubber compound, fracture mechanics, crack, initiation, growth, fracture, fatigue, wear, mechanical loads*

Plná verze disertační práce je dostupná v Knihovně UTB ve Zlíně.

ISBN 978-80-……

Content

Abstract

The thesis deals with fracture behaviour of rubber and methodology associated with its characterization. Understanding particular mechanisms of fracture is important in prediction of rubber compound performance under real loading conditions and increase of rubber products service life. The theoretical part summarizes published approaches used to characterize fracture behaviour of rubber. In addition, a part of theoretical background is devoted to the analysis of fatigue crack growth (FCG) and describes the effect of the structure and test conditions. The experimental part focuses on the preparation of rubber compounds based on natural rubber (NR), butadiene rubber (BR) and styrene butadiene rubber (SBR) as well as combinations of them. Subsequently, rubber test specimens are prepared for characterizing the fracture behaviour throughout their service life under cyclic and static loading. Last but not least, functional prototype of device for characterization of the fracture behaviour of stressed rubber in tension simultaneously being penetrated by sharp object is introduced.

Keywords: rubber, rubber compound, fracture mechanics, crack initiation, crack propagation, fracture, fatigue, wear, mechanical loads

Abstrakt

Předložená práce se zabývá problematikou lomového chování pryže a metodikou spojenou s jeho charakterizací. Pochopení mechanismů jednotlivých stádií lomu je důležité z hlediska predikce a zvýšení doby životnosti pryžových výrobků v reálných podmínkách. V rešeršní části práce jsou shrnuty teoretické přístupy užívané pro charakterizaci lomového chování pryže. Mimo to je pozornost věnována rozboru únavového lomu a popisu vlivu struktury a zkušebních podmínek na jeho průběh. Experimentální část je zaměřena na přípravu kaučukových směsí na bázi přírodního (NR), butadienového (BR) a styren butadienového (SBR) kaučuku, tak jako jejich kombinací. Z připravených kaučukových směsí byla vyrobena pryžová zkušební tělíska pro zkoušky charakterizující lomové vlastnosti v jednotlivých stádiích životnosti při cyklickém a statickém zatěžování. Mimo to byl představen funkční prototyp zařízení schopného charakterizovat lomové chování pryžového tělesa namáhaného tahem, do něhož současně vniká ostrý předmět.

Klíčová slova: pryž, kaučuková směs, lomová mechanika, iniciace trhliny, propagace trhliny, lom, únava, oděr, mechanické zatížení

1. INTRODUCTION

Rubber-like materials are widely used in engineering applications because of their unique properties that combine high extensibility, high strength, high energy absorption and high resistance to fatigue and good environmental resistance. [1] Elastomers, which provide major influence on these properties, are amorphous polymers consisting of simple molecules, known as mers. [2] Mechanical properties of an elastomer compound change during a chemical process called vulcanization. During vulcanization, rubber acquires its unique properties. Cured rubber can reach values of extension ratio up to 1000 % based on type of rubber. In addition, vulcanization extends service-life over a great range of temperature. [3 – 5] Thousands of products such as tires, hoses, belts, seals, bearings and bushings are manufactured using such types of rubber. Indeed, rubber is crucial for a modern industrialized economy because of its wholesale usage *e.g.* in the automotive industry. In fact, a modern passenger car contains over 600 rubber parts. [6] Rubber products are exposed to large static and time-varying strains over a long time. Long-term durability is therefore a critical issue. The mechanical fatigue and the nucleation and growth of cracks in the rubber are very important aspects influencing products' service life. For effective and economical solution of mechanical fatigue issues, engineers need to model and design the product development process in accordance to the state of the art requirements for rubber products. [7] The theoretical background of this work gives a summary of the various theoretical approaches describing fracture mechanics, especially approach based on the energy balance of the system. Experimental part deals with the description of fracture behaviour during various stages of tearing level. In order to describe fracture properties of commonly used elastomers and their blends, several fundamental mechanical methods based on the energy balance were used. Moreover, new methodology and testing prototype able to characterize minimal energy for crack growth has been introduced.

The aim of this work is a thorough description of several types of fundamental testing methods and their application. The methods are based on varied loading conditions in order to investigate complex fracture properties from crack initiation up to total rupture of basic commonly used vulcanizates, which are based on natural and synthetic elastomers. However, the main mission is to elaborate simple but very complex overview over state of the art testing methodologies and equipment leading to the predicative description of fracture behaviour of rubber products with respect to the real loading conditions occurring in service life and thus summarize a prescription for simple, smart and efficient fracture characterization in a laboratory.

2. THEORETICAL BACKGROUND

2.1 Fatigue of rubber-like materials

Mechanical fatigue in rubbery materials is demonstrated by a progressive weakening of physical properties as a result of crack growth during application of dynamic loads or deformations. [8] The process of mechanical fatigue can be divided into four stages, which characterize different phases of tear behaviour. The initial process of tearing describes a generation of high stress concentration around area of natural defects or flaws. In the second stage, the crack initiation occurs due to formation of defects at a molecular level. In another stage, the formed crack grows due to additional load. The mechanical fatigue in a limiting case leads to failure. [9] Many factors influencing the mechanical fatigue life of rubber components are known. The four major aspects are effect of mechanical loading history, environmental effect, effect of rubber formulation, and effect due to dissipative aspects of the constitutive response of rubber. [10] Recent research into the fatigue of rubber has focused on the mechanics of fatigue failure as well as on the development of the complete fracture process. [11] The primary significance has description of local stress concentrations around structural flaws. Hence, the fracture mechanics approach has been evolved. [8]

2.1.1 Crack Initiation

Crack initiation is a localized deformation process that is necessary for crack propagation. [12] One of the necessary premises of fracture mechanics is the presence of natural defects or flaws, which form highly localized stress concentrations that initiate failure at fatigue loading. [8] Under sufficient magnification, every solid body contains heterogeneities of composition or structure, each of which may serve as the precursor to a crack. [3] For natural rubber, the size of flaws which can cause initiation of crack is estimated to be about 25 μm. Another precursor to mechanical fatigue is a crack initiated by ozone at surface areas where tensile stress is present. [8] The degree of crack initiation resistance can be defined as the number of cycles required to cause the appearance of a crack of a certain size. A. Wohler introduced the first known study regarding this topic in 1860. Wohler's study dealt with railroad axles. A similar analysis approach was applied to rubber characteristics experiments in 1940 and has been used since. [13] Two parameters are widely used for a detailed prediction of crack nucleation in rubber i.e. maximum principal strain or stretch, and strain energy density. The strain analysis is a common investigative tool because it can be directly determined from an immediate tensile test measurements of displacements. When strain energy density is applied to evaluation of fatigue analysis in rubber, it is often estimated from a hyper-elastic strain energy density function, which is defined entirely in terms of strains. [14] The energy release rate is proportional to the strain energy density and the crack size at certain conditions and far from the crack. [15, 16] When

the above mentioned conditions are reached, the strain energy density is a measure of the energy release rate of naturally occurring flaws. The conditions under which the strain energy density may be uniquely related to the energy release rate are limited. For the relationship to hold, it is assumed that crack growth is self-similar, that the far-field strain gradient across the crack is negligible, and that the stress state is one of simple tension. [7]

2.2 Fracture mechanics

The fracture mechanics is a branch of science that deals with description of material behaviour containing a notch. It includes methods for calculating mechanical characteristics such as crack driving force and resistance to fracture. Fracture mechanics is an important tool for mechanical performance improvement of materials and components that defines relationship between stress and strain by using the theories of elasticity and plasticity of materials. Indeed, it is a quantitative analysis for evaluating structural strength depending on applied stress, crack length, and specimen geometry. [4]

Fundamentals of fracture mechanics were laid by an English aeronautical engineer, Griffith, during World War I. In 1920 Griffith quantitatively connected the strength and crack size for brittle materials. Griffith's theory is based on energy-balance approach that describes the slow propagation of a crack as a conversion of elastic energy stored in the bulk to surface energy. Griffith postulated that the strain energy of the material decreases at constant deformation due to creation of new fracture surfaces. [11, 17, 18]

$$U = U_0 - U_a + U_\gamma \tag{1}$$

Energy balance is given by Equation 1 where U represents potential energy of the system, U_0 is potential energy of the system before introducing the crack, U_a (strain energy) and U_γ (surface energy) decreases in potential energy due to deformation associated with introduction of the crack and increase in surface energy due to the newly created crack surfaces, respectively. [19]

Progress of the individual energy components is dependent on crack size, a is illustrated in Figure 1. Potential energy of the system is consumed during crack propagation and decreases by the square. On the contrary, the surface energy of the newly formed surface increases linearly. The critical length of crack denotes a point where potential energy of the system declines. A crack that has length less or equal to critical length is not spread without addition of external energy. [20]

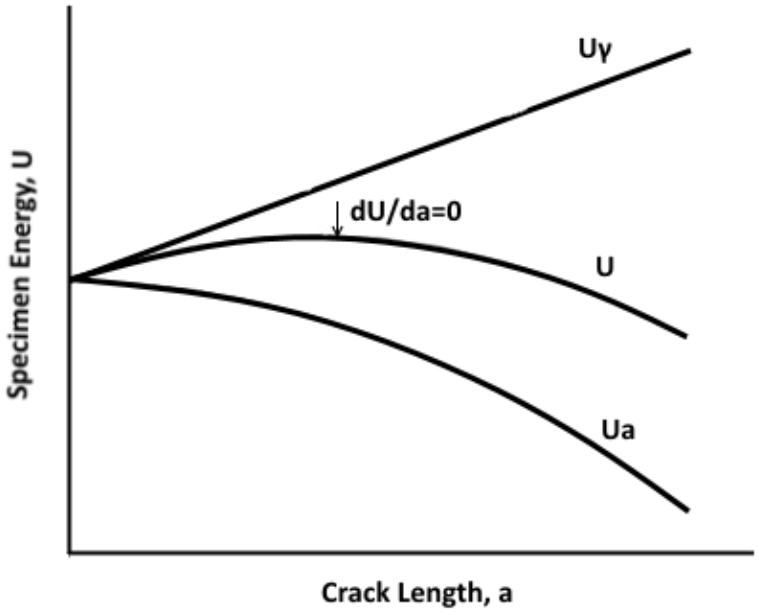

Figure 1. Dependence of energy components on crack length.

Griffith's original work dealt with very brittle materials, specifically glass rods. Therefore, it cannot be applied to describe the behaviour of ductile materials e.g. metals. Irwin and Orowan independently proposed extensions of the Griffith's theory to make it usable for ductile materials almost 30 years after Griffith. They pointed out that for engineering materials the strain energy is not absorbed only to create new surfaces but the energy is also dissipated due to plastic flow in the material close to the crack tip. They suggested that crack growth occurs when enough strain energy for both processes required to crack propagation in ductile materials is released. [10, 20, 21] However, fracture behaviour is characterized by relationship between crack driving force and crack resistance.

2.2.1 Crack driving force

Crack driving force *G* is proportional to the energy available for fracture, and is equal to the mechanical work necessary to increase crack area per unit and can be written in following form,

$$G = -\frac{dU_a}{dA} \tag{2}$$

where U_a is strain energy and *A* is area of newly created crack surface.

2.2.2 Crack growth resistance

The crack resistance *R* is a material constant which characterizes the amount of energy necessary to allow propagation. The degree of resistance against crack growth is given by value of material surface energy U_γ.

$$R = \frac{dU_\gamma}{dA} \tag{3}$$

Generally, the crack driving force increases with crack length so that after initiation, unless there is a similar increase in resistance, there is a positive difference between driving force and resistance and more energy is available for fracture than is required simply to create the new fracture surfaces. [22] There are two ways, depending on the ratio between value of driving force and crack resistance, how crack can spread after exceeding the critical value.

Steady state crack propagation

$$\frac{dG}{dA} \leq \frac{dR}{dA} \tag{4}$$

Unsteady state crack propagation

$$\frac{dG}{dA} > \frac{dR}{dA} \tag{5}$$

2.2.3 Stress intensity factor

In 1957 Irwin has developed stress intensity factor which is one of the most fundamental and useful parameters in fracture mechanics. The stress intensity factor *K* is used to predict stress intensity around an elliptical crack in linear elastic material under tension and can be applied to materials that exhibit small-scale yielding at a crack tip. The value of *K* is dependent on specimen geometry, an amount and distribution of load on the material and the size and location of the crack. To obtain sufficient accuracy the crack depth should be less than a half of a specimen thickness and yielding should be restricted to a small zone at the crack tip. [23, 24] The stress intensity factor in tension is given by Equation 6, where σ describes tensile stress, a is crack length and d denotes thickness of specimen.

$$K_1 = \sigma\sqrt{\pi a}\, f_1\left(\frac{a}{d}\right) \tag{6}$$

This approach is fully applicable to materials having linear mechanical behavior because of this reason it is not well suited for the determination of the fracture behavior of rubbers due to their viscoelasticity.

2.2.4 J-integral

The fracture mechanics was extended by J-integral which theoretical concept was developed for non-linear elastic materials in 1967 by Cherepanov and in 1968 by Rice, independently. J-integral is a parameter that successfully characterizes stress and strain fields around the crack tip in static and steady-state dynamic load and can be applied for determination of material that exhibits significant plasticity and deals with elastic behaviour of material, too. The integral is widely used as a criterion for comparison of fracture behaviour of different materials. Rice showed that an energetic contour path integral was independent of the path around a crack. The J-integral approach characterizes

the fracture properties by assuming that a critical amount of energy is required to advance a crack by unit area. Lee et al. found out that the J-integral approach exhibited less scatter than the tearing energy approach but required a larger crack length versus specimen length ratio to obtain accurate values. Furthermore, the J-integral technique separated the critical energy in the region of the crack tip and the stored elastic energy in the bulk. Lee et al. recommended that the critical crack tip energy release rate for initiation and fracture to be considered material properties, which represent the material resistance to fracture as well as being an appropriate parameter for material evaluation. [11, 25 – 28] J-integral is determined by Equation 7,

$$J_k = \int_{r_0} \left(w n_k + \sigma_{ji} n_j \frac{\partial u_i}{\partial x_k} \right) ds \tag{7}$$

where, *w*, is the strain elastic energy density, *n* is the outer normal unit vector of r_0, σ is the stress tensor, *u* is the displacement vector and *s* is the element length. Nowadays J-integral approach is becoming more important for characterization of fracture behaviour. However, characterization based on the energy balance of system according to Griffith's theory is still popular due to its simplicity.

2.3 The fracture mechanics of rubber

The Griffith's concept for a crack growth inside brittle materials does not represent exactly the fracture mechanics of rubber due to its viscoelastic behaviour. The stored elastic energy in the bulk serves as a driving force *G* of crack spreading in rubber and its amount required to growth a fracture surface by one unit area characterizes mechanical strength of elastomers. Viscoelastic zone in vicinity of crack tip leads to the fact that amount of *G* does not depend only on energy necessary to break bonds at crack tip, but also on energy dissipated in vicinity of crack tip during crack propagation. Experiments [29] [30] have shown that *G* depends on the crack-tip velocity *v* and on the temperature *T* in accordance with

$$G(v,T) = G_0[1 + f(v,T)] \tag{8}$$

when f → 0 as v → 0, the value of *G* is equal to threshold value G_0 which is represented by no fracture occurrence. For non-crystallizing elastomers, the value of *G* evaluated at extremely low crack velocities and high temperatures, when viscous effects in the rubber are minimized is equal to G_0 whereas at high crack velocities *G* may be up to 10^4 times higher. [31]

When crack tip velocity is so slow that growth of temperature at crack tip can be ignored, the effect of temperature can be characterized by applying a simple multiplying factor aT to the crack velocity. Determination of aT can be

performed experimentally using Williams-Landel-Ferry function from temperature dependence on the bulk viscoelastic modulus. [32]

$$\log \quad aT = \frac{C_1(T-T_g)}{C_2+(T-T_g)} \tag{9}$$

where C_1 and C_2 are two constants and T_g is the glass transition temperature of the rubber type.

According to this relation, it is obvious that the effects of crack velocity and temperature on crack propagation in rubber materials are due to viscoelastic processes in the bulk. [33]

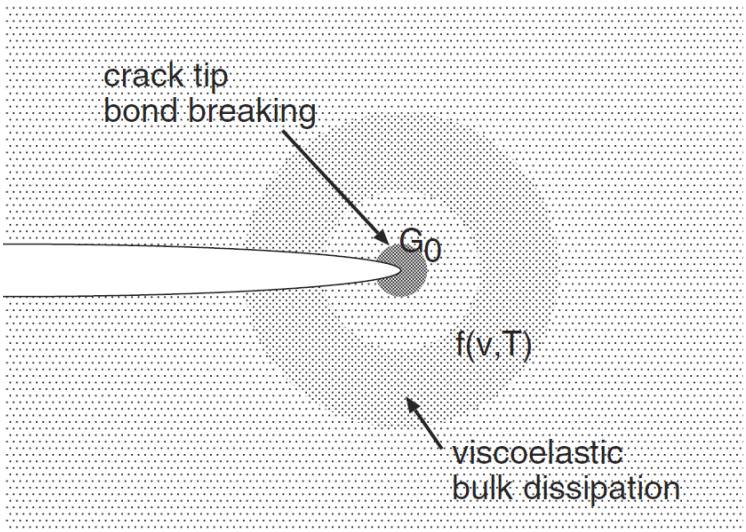

Figure 2. The crack propagation energy G is a product of a term G_0 derived from the bond breaking at the crack tip, and a term f (v, T) derived from the bulk viscoelastic energy dissipation in front of the tip. [31]

Stresses induced at the tip of a crack in viscoelastic solid cause large local deformations which lead to dissipation of energy. The innermost region at the crack tip zone is associated with highly nonlinear processes like cavity formation and bond breaking. This region is in glassy state for high frequencies $\omega = v / r$ (high crack velocities v and short distance from crack tip r) and is described phenomenologically via the term $G_0 = 2\gamma_0$ where for rubber-like materials γ_0 is much larger than the surface energy γ. The elastic modulus of glassy region is $E_{(\omega)} \approx E_\infty$. The second contribution comes from the viscoelastic dissipation in the polymer in the linear viscoelastic region in front of the tip which is given by factor $f(v,T)$ and it is referred to as transition region which exhibits the highest values of loss factor. For a fast moving crack this may be very far away from the crack tip. The last region which is represented by rubbery behaviour where $E_{(\omega)} \approx E_0$ is indicated for large distance r. When a crack

propagates in a viscoelastic material, heat is produced in the vicinity of the crack tip, which will increase the temperature close to the crack tip. For fast crack propagation flash temperature effect leading to increase of temperature close to the crack tip is visible. This effect is caused due to a movement of a crack tip from the glassy region which contributes very little to the total energy dissipation towards the transition region where viscoelastic energy dissipation occurs. [31]
The crack will propagate when energy required to create the new surface plus the energy required by the viscoelastic dissipation processes near the crack tip is supplied to the system. The strain energy release rate criterion is still valid for rubber materials, when the energy dissipation is confined to a small zone at the crack tip. [8, 33] Rivlin and Thomas were first to apply Griffith's theory to the tearing of rubber successfully. [34] Rivlin and Thomas developed a criterion for the tearing of a rubber vulcanizates, which is analogous to the Griffith's characteristic energy, describing the amount of energy released per unit area of crack surface growth, i.e. the tearing energy T that is defined by Equation 10 [35] [36]

$$T = -\left(\frac{dU}{dA}\right) \tag{10}$$

where U is the elastic energy of specimen and A is the area of the created fracture surface.

The energy necessary to grow the crack is supplied either from the strain energy in the deformed rubber, or as energy applied by mechanical loading or both. When the tearing energy T exceeds the value T_{cr} crack growth will occur. It is evident from the experimental results that critical value of the tearing energy is independent on the geometry and dimensions of the specimen and can be considered as a material property. For component design the tearing energy, T, is calculated for a hypothetical crack and compared with T_{cr} to determine the criterion for the crack propagation. [35]

Because of the nonlinear behaviour and large deformation, it is difficult to determine the tear energy using applied forces or deformations. However, by suitably choosing the specimen geometry the tearing energy can be determined without detailed knowledge of strain energy density. Thomas showed that the tearing energy is given by Equation 11,

$$T = W_b \cdot d_n \tag{11}$$

where W_b and d_n are work required to break and diameter of notch tip, respectively. [37]

2.3.1 Types of specimens used for determination of tearing energy

In the literature there are a few methods frequently used to calculate tearing energy. Those differ in a type of specimen used. Each of these types has some limitation in testing and it is important to understand them.

Trousers-tear test specimen

The trousers-tear specimen has become a favorite test piece for determination of anti-plane-mode critical tearing energy for elastomers. The specimen has a rectangular shape that is cut lengthwise to form two legs which are pulled in opposite directions out of the plane of the test piece by equal and opposite forces. [35] Tearing energy is calculated by

$$T = \frac{2\alpha F}{t} - bw \tag{12}$$

where α is extension ratio, F is tensile force on the leg, b is total width of specimen and w is strain energy density.

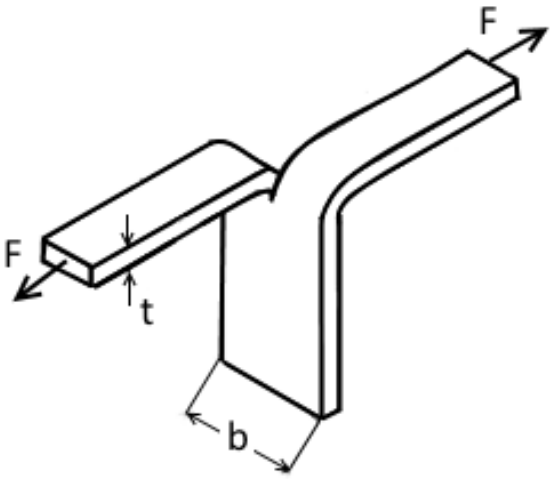

Figure 3. A scheme of trousers-tear test specimen.

Single edge notched tension (SENT) test specimen

SENT test specimen is represented by one side notched strip that is loaded in tension. It is important that the crack length is small compared to the width of sample and the tip of the crack is far enough from the free edge opposite the crack. [38, 39]

$$T = 2\frac{\pi}{\sqrt{\alpha}}wa \tag{13}$$

with α is extension ratio, a is crack length and w is strain energy density.

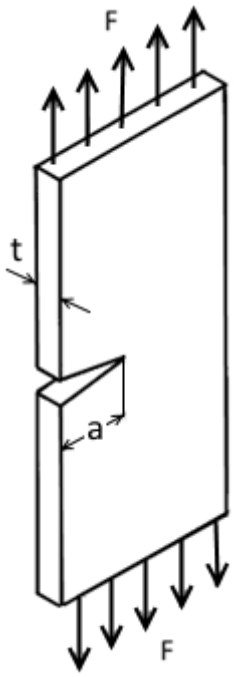

Figure 4. A scheme of a SENT test specimen.

Pure-shear test specimen

The pure-shear specimen is a wide strip of rubber material that contains a long edge crack. Usually the notch length is sufficiently long compared to the length of test specimen. The test specimen can be divided into different regions that are shown in Figure 5.

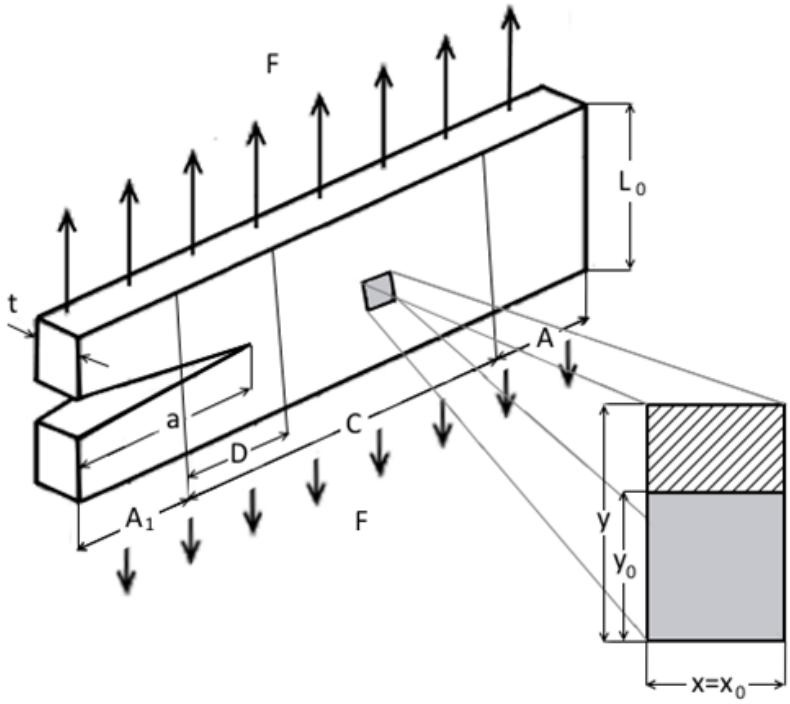

Figure 5. A scheme of pure-shear test specimen.

Region A_1 is represented by presence of notch and strain is not exhibits. Region C-D is in pure-shear state, whereas the region C is identical with the pure-shear state region in the un-notched test specimen geometrically defined as follows:

$$\lambda(x) = \frac{dx}{dx_0} = 1$$

$$\lambda(y) = \frac{dy}{dy_0} = \frac{y}{y_0} = \varepsilon(y) + 1$$

$$\Rightarrow \quad \begin{bmatrix} x \\ y \end{bmatrix} = \begin{bmatrix} 1 & 0 \\ 0 & \varepsilon(y) + 1 \end{bmatrix} \cdot \begin{bmatrix} x_0 \\ y_0 \end{bmatrix} \qquad (14)$$

Region D exhibits complicated strain around the crack tip. The increase of crack length by *da*, induces the movement of the region D along the *da*, but the pattern of strain, and hence the energy stored remains unaltered. For a pure-shear test geometry the tearing energy *T* is considered to be independent of the crack length and it is given by: [36]

$$T = wL_0 \qquad (15)$$

where *w* is strain energy density and L_0 is initial length of the specimen.

There is no direct way how to calculate the strain energy densities from the tearing test. The strain energy density has to be obtained by a separate test on an uncut specimen or developed from a finite element analysis. It is necessary to realize that the value of strain energy density is dependent on conditions of testing because its value decreases with time or cycles due to stress relaxation. [38]

In Figure 6 four different measurements of force vs. time during tearing of notched specimen are represented. The steady state tearing which is characterized by smooth shape of force versus time measurement and only limited change of crack growth rate is shown in Figure 6 (a) and (b). Certain types of elastomers exhibit stick slip effect as shown in Figure 6 (c) or even knotty in behaviour as shown in Figure 6 (d). These phenomena represent unstable tearing and rate of crack growth is much harder to determine due to fluctuations between a very rapid rate and a zero rate of crack growth. [40]

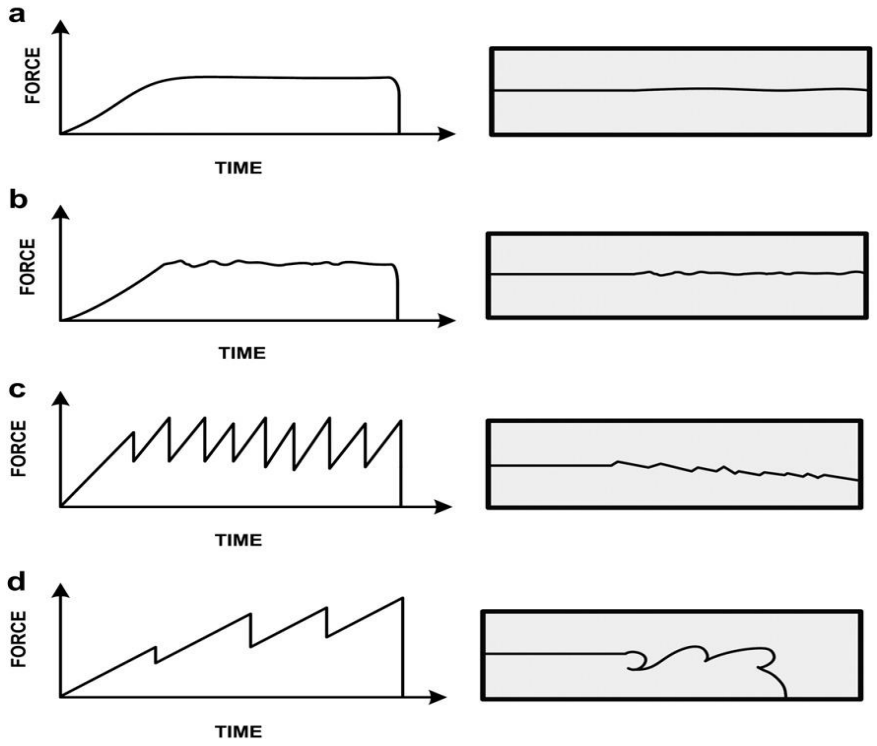

Figure 6. Schematic diagrams illustrating the tearing force time relationships and tearing path for different types of crack propagation obtained from the trouser tear specimen: (a) and (b) steady tearing, (c) stick-slip tearing and (d) knotty tearing. [40]

2.4 Crack propagation during fatigue life

Most of rubber products are stressed by cyclic loading that leads ultimately to failure of the product. The fatigue life of the product is determined by the number of cycles under a declared test condition that can be performed before a failure occurs. [41] There are many factors to influence the fatigue behaviour of rubber. Four general classes of factors are mechanical load history, environmental conditions, formulation of the rubber compound, and dissipative aspects of the stress-strain behaviour. [42] The fatigue life is normally determined from experimental data by a "Wohler" curve, also known as an S-N curve where S denotes the applied dynamic stress for a stress-controlled test or, alternatively, strain for a strain-controlled test, and N is the number of cycles to failure. Experimental determination of fatigue life of samples without notch shows a large scatter in the final fatigue life. In addition, these measurements are very time consuming therefore useless in terms of usability in industry. The obtained information is corresponding only for the specific test specimen, which may not be representative of the typical components in service. [8]

Many experimental methods determine the fatigue crack growth rate over a wide range of tearing energies and from their results a relationship between crack growth rate and fatigue can be established.

2.5 Methodology of fatigue crack growth testing

As already mentioned, there are many factors affecting the fatigue process in rubber and it requires many approaches to analyse fatigue behaviour.

2.5.1 Effect of mechanical loading

Experimental analyses based on mechanical load are most common. By definition, mechanical fatigue involves crack nucleation and growth due to fluctuating loads. The driving force of load can be represented by any of various parameters associated with specific analysis approaches: strain, stress, strain energy density, energy release rate, etc. The value of mechanical loading is usually determined as maximum, alternating, minimum and mean loading, and/or the R-ratio. [42] Widely used rubber fatigue tests monitors the behaviour of the material under alternating load which cause fatigue failure even at lower levels of load than static load. Although static loads do not cause fatigue failures even at high levels it can cause failures due to steady, time-dependent crack growth in the case of elastomers that do not exhibit strain crystallization, or in the presence of environmental attack. [42] In Thomas fatigue crack growth approach, crack growth rate against the maximum energy release rate attained during the cycle was arranged. This relationship is known as the crack growth characteristic of the material because it is independent on the piece geometry. [43] Typical curves for a natural rubber and a styrene-butadiene rubber are shown in Figure 7. The applied history in that work was fully unloading cyclic tension (R = 0).

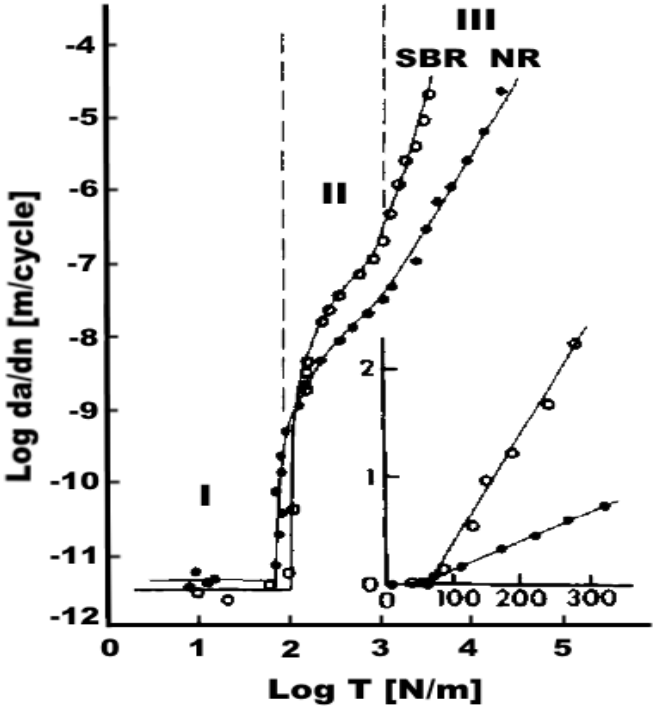

Figure 7. Visualization of crack growth progress rate under cyclic loading, for unfilled NR (•) and SBR (o) compounds, as a function of the tearing energy of the cycle. [8]

The course of crack growth rate can be divided into four regions. In the first region the value of tear energy T is under threshold of tear energy T_0 and no mechanical crack growth occurs. Under T_0 mechanical failure may be caused by other factors, e.g. ozone. This region is described by

$$\frac{da}{dn} = R_z \tag{16}$$

where R_z is crack growth due to ozone attack. [44]

In the second region visible synergistic effect of environmental and mechanical factors on crack growth rate is visible which is given by

$$\frac{da}{dn} = R_z + A(T - T_0) \tag{17}$$

where A is crack growth constant for region II.

In region III, the power law is observed between crack growth rate and T. This shape of dependence often occurs in fatigue crack nucleation tests (load vs. life) and in fatigue crack growth tests (load vs. crack growth rate). An analytical relationship between fatigue crack growth tests and crack nucleation tests in this regime has been derived. Thus,

$$\frac{da}{dn} = BT^F \tag{18}$$

where B and F are constants characteristic of region III. [15] For NR F is about 2, whereas for SBR is about 4. [8]

In the last region, the value of T exceeds a critical value and the crack growth rate accelerates rapidly to unstable fracture. Crystallizing rubbers containing a small crack exhibits strain crystallization before the point of unstable crack growth at high strains. [44]

Description the crack growth rate under cycles which are not fully unloaded (R > 0) is another approach commonly used in service. In service the load is rarely fully unload, in contrast to typical laboratory studies. The effect of minimum or mean loading on fatigue life depends on polymer and filler types. There is important difference between the crack growth behaviour of strain induced crystallizing and non-crystallizing rubbers. Non-crystallizing rubbers can exhibit steady crack growth under static loading therefore crack growth rate under cyclic load is given by sum of contributions of steady and cyclic crack growth rate behaviour. Whilst crystallizing rubbers typically exhibit no crack growth because of the formation of crystalline zone in front of the crack tip leading to deviation of the crack path from orthogonal direction of main strain. This property is characteristic for NR that exhibits strain induced crystallization. Whereas at fully unloaded mode (R = 0), these crystallites disappear during

every unloading cycle as the samples will be totally in strain free condition. [42, 45, 46]

2.5.2 Effect of loading waveform shape

Waveform shape of loading has an influence on fatigue behaviour, particularly for amorphous polymers. It is also important to adjust the waveform shape to service load conditions corresponding with tested product. In several researches dealing with fatigue crack propagation, sinusoidal waveform was used, which is considered more realistic to the strain history in a tire that is one of the most manufactured rubber products. For instance, dual-sine waveforms occur in engine mounts. However, the effect depends not only on polymer type, but also on other compound ingredients. Hardy et. al. in [47] found that amorphous bromobutyl (BIIR) rubber for certain types of filler exhibits a different order of magnitude crack growth rates under pulse and sine waveforms. The pulse waveform leads to higher crack growth rates than sine waveform at same peak energy release rate because the loading rate in the pulse waveform is much greater than the loading rate in the sinusoidal waveform. [8, 42, 47] Higher loading rate leads to instantaneous increase of crack tip temperature and in turn higher crack growth rate. This phenomenon is associated with the viscoelastic energy dissipation process at the crack tip as explained by Persson et. al. [31] The movement of polymer molecules becomes easier due to decrease of intermolecular chain friction that results in decrease in viscous dissipation at elevated temperature. [48] Gosh et al. [49] investigated that the relaxation time between pulses has an influence on crack growth rate. According to this research, a higher relaxation time may reduce the crack growth rate due to decrease of temperature at the crack tip.

2.5.3 Effect of loading frequency

The effect of loading frequency depends on polymer type. Large effect of frequency has been observed for amorphous polymers because of time-dependent continuous crack growth, associated with viscoelasticity. This steady component of crack growth is especially important at frequencies below about 0,2 Hz. Natural rubber shows very little effect of frequency on fatigue cracking over the range of 10^{-3} to 50 Hz. High levels of frequency cause the generation of heat in material, especially for thick samples where heat degradation is predominant reason of failure. This type of failure called thermal runaway often occurs in tires where leads to blowout of tires which are exposed to high speed or overload. [44, 50, 51]

2.5.4 Effect of rubber formulation

The rubber compound consists of a broad range of ingredients. Mechanical properties can be improved by varying type or quantity of each ingredient. The

biggest influences on fatigue behaviour are polymer type and filler type. Manufacturing processes also affect fatigue behaviour through their influence on factors such as ingredient dispersion, state of cure and the presence and nature of precursor sites for crack initiation. [42]

2.5.5 Effect of rubber constitution

In real application many types of elastomers with different level of viscoelasticity is used. It has been proven that viscoelasticity influences steady state crack growth rate in amorphous elastomers. Mullins [52] found a simple proportionality between loss modules and the energy release rate at a given crack growth rate. This theoretical assumption was confirmed by Ahagon et. al. [53] who performed tear measurements at low crack velocity for unfilled butadiene rubber and styrene butadiene rubber. It was find out that the energy necessary to crack propagation is lower for butadiene rubber exhibiting lower values of loss modules in comparison with styrene butadiene rubber. Thus material exhibiting higher loss modulus requires a higher energy release rates to drive a crack at low crack tip velocity. [51] In Figure 9 it is shown the summary of FCG behaviour of commonly used elastomers filled by high and low reinforcing carbon black and compared to the corresponding unfilled elastomers. Some types of elastomers exhibit ability to strain induced crystallization. These elastomers are perfectly dissipative at high strains and have good resistance to crack propagation until the stress is so high to rupture. For crystallizing elastomer types, it is necessary that time to relaxation of polymer chain must be shorter than time for stretching a polymer chain at the crack tip. The minimum value of power-law fatigue crack growth constant F (Equation 18) is about 2. This is because the stress distribution for a sharp crack leads to growth steps that depend on the square of the tearing energy. [54] For relatively elastic materials, F should be significantly greater than 2, approaching infinity for a perfectly elastic solid. Some of elastomers that exhibit strain crystallization are natural rubber, isoprene rubber (IR) and polychloroprene (CR) whereas styrene-butadiene rubber, polybutadiene, butyl rubber (IIR), acrylonitrile-butadiene rubber (NBR) and ethylene-propylene rubber (EPDM) exhibit little or no crystallization. The effect of strain induced crystallization is time dependent. When the strain is reduced sufficiently, the crystallized structure returns to the amorphous state. In strain crystallizing rubbers, steady crack growth under a static load is usually not observed. Steady crack growth is usually observed for non-crystallizing materials. [15, 55] It is caused by inhomogeneous nature of rubber. In Figure 8 it is shown the bond-breaking process at crack tip in rubber occurring no strain crystallization (left) and rubber with ability to strain crystallization (right). Because of the inhomogeneous nature of rubber, different polymer chains at the crack tip will be stretched to the break limit at different times. For rubber which exhibits strain crystallization (right), the chains in the vicinity of a fully stretched chain will adhere in commensurate way to the

stretched chain, thus strengthening the weakest link. This will result in a strong enhancement in stress at the crack tip necessary for the onset of crack propagation. [31] Moreover, values of *F* are not dependent only on strain level but also on strain rate. Elastomers that exhibit strain crystallization have a lower fatigue crack growth exponent *F*, and are superior at high strain rates, relative to other elastomers. NR is the most resistant material at high tearing energies rate and NBR is the worst. In contrast, at lower tearing energies, CR is significantly better than NR.

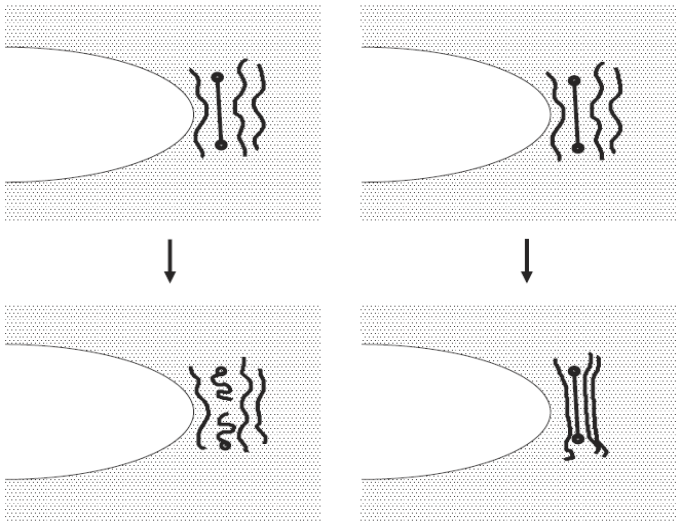

Figure 8. The bond-breaking process at crack tip in rubber. [31]

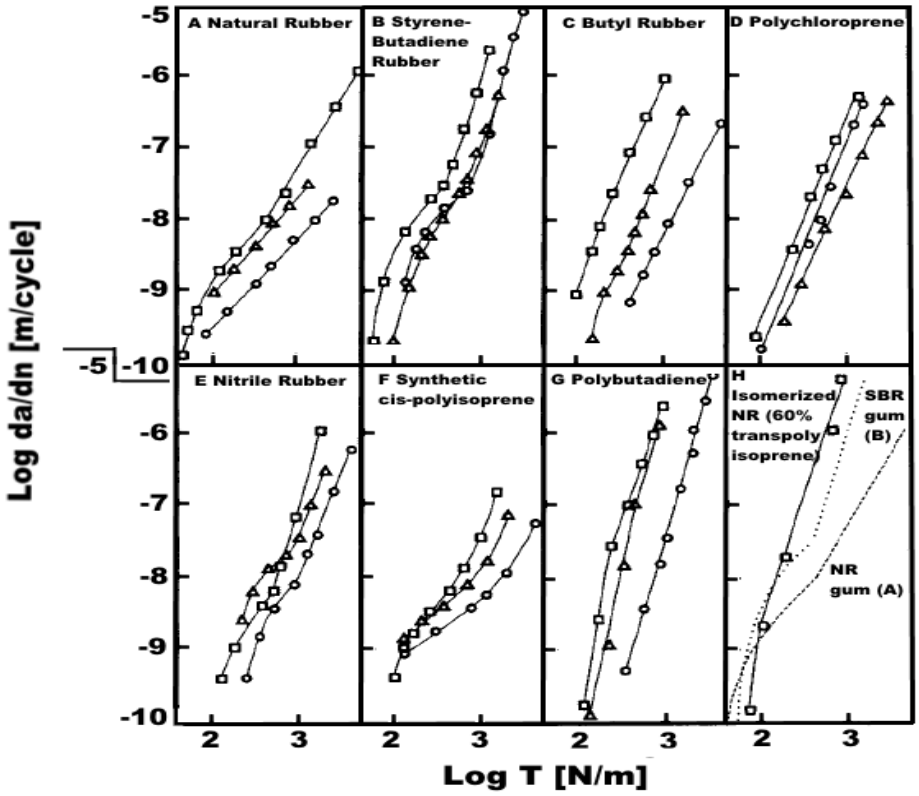

Figure 9. Crack growth characteristics of vulcanizates from different compounds: □, gum; Δ, with 50 phr N900 carbon black;○, with 50 phr N300 carbon black. [8]

2.5.6 Effect of fillers

The presence of carbon black in the material influences fatigue behaviour. Furthermore, carbon black serves as a protection against ultraviolet degradation. Resulting effect depends on type and volume of filler. The effect of filler on fatigue properties has been attributed to multiple mechanisms like change on stiffness and hysteresis properties. Moreover, carbon black has the ability to change crack growth rate due to deviation and branching, induced by nonhomogeneity at crack tip. Filled rubber compounds exhibit the Mullins effect characterized by an initial transient softening of the stress-strain dependency. [56] The improvement of fatigue properties of filled non-crystallizing elastomers has been attributed to this dissipative mechanism. [8] There are two types of carbon black. One of them is high reinforcing High Abrasion Furnace (HAF) black, which considerably improves the cut growth resistance of all the vulcanizates except CR, and low reinforcing Medium Thermal (MT) black which has a beneficial effect on SBR, butyl, and CR. At low tearing energies, close to the fatigue limit, reinforcing fillers increase the value of T_0 by about 50%. [55] The volume fraction of filler is necessary to choose depending on required properties of materials. High volume of filler leads to changes in the stiffness and hysteresis of the material, which may lead to heat buildup, which may promote further fatigue cracking. [9]

2.5.7 Effect of thermal aging

During service life, rubber components may be exposed to higher temperature that causes chemical changes in rubber material, which results in the deterioration of mechanical characteristics. Thermal aging has impact to crosslink density that determines the physical properties of a vulcanizate. Increasing crosslink density increases elastic modulus, hardness, resilience, and abrasion resistance, whereas the elongation at break, heat build-up, and stress relaxation decrease. Rubber compounds are cross-linked by several types of chemicals such as peroxide, resole cure system or sulphur which is the most popular cure agent. [57] The process of crosslinking involves three types of crosslinks in the vulcanization: polysulphide, disulphide and monosulphide. The bond energy between the sulphur crosslink atoms and the polymer backbone depends on the type of bond. Polysulfide bonds are the most susceptible to decomposition by heating that may occur at considerably lower temperatures than the decomposition of the main chains. [58] As an alternative, the peroxide curing system has been used to overcome this problem. The thermal stability of C-C linkages improves the ageing properties of elastomer compounds. [59]

The crosslink density increases due to the presence of unreacted curatives in rubber matrix upon thermal aging. In general, crosslink density of a sulphur-cured rubber vulcanizate increases with increase of the aging temperature.

However, for a rubber vulcanizate with an elemental sulphur-free cure system the crosslink density after thermal aging at high temperatures decreases. [57]

Elevated temperature has a detrimental influence on the fatigue behaviour both on crack nucleation and to crack propagation. [42] The amorphous elastomers are most affected. For SBR in displacement-controlled tests, fatigue life drops by a factor of 10^4 as the temperature increases from 0 °C to 100 °C. [55] For NR in displacement-controlled tests, fatigue life drops by a factor of only 4, for the same temperature range. The incorporation of fillers may reduce the temperature dependence slightly. [60]

3. AIMS OF THE WORK

The aim of the work is contribute to the field of characterization of fracture behaviour of rubber. Rubber compounds contain a wide range of ingredients which influences their final properties. Moreover at real conditions of usage, rubber products are mechanically loaded in a various ways that affect their fracture behaviour. For a fundamental prediction of lifetime of rubber products is necessary to understand interrelations between structure and mechanical loading and their influence on fracture behaviour.

Thus, the main goal of the study is experimental determination of the interrelations between structure and loading condition on fracture behaviour. Natural rubber and two wide used synthetic elastomers were used for determination of fracture behaviour.

The aims of this work have been summarized in the following major points:

- Preparation of carbon black filled rubber compounds based on NR, BR, SBR and their combination.

- Determination of mechanical properties using basic testing methods.

- Creation of overview of basic test methods characterizing the fracture behaviour of rubber in quasi-static, dynamic or cyclic loading, supplemented by results.

- Introduction of functional prototype of a device which is able to characterize the fracture behaviour of rubber, supplemented by results.

4. EXPERIMENTAL PART

During service life, rubber products are rarely visibly loaded in tension. However, from the mechanical point of view the tension is one of the main stress vectors of a loaded element. Figure 10 schematically shows bending of beam where the tension is clearly illustrated. Therefore, for the fundamental understanding of mechanical as well as fracture behaviour of material it is important to perform experimental investigation in tension. Stoček et al. [61] showed the correlation between the tensile fatigue crack growth analyses and real tire test on drum testing equipment. This chapter covers the experimental setup of procedures which were used to describe fracture behaviour of vulcanizates. All these experimental procedures are completed by results of fracture behaviour of prepared vulcanizates based on natural and synthetic elastomers.

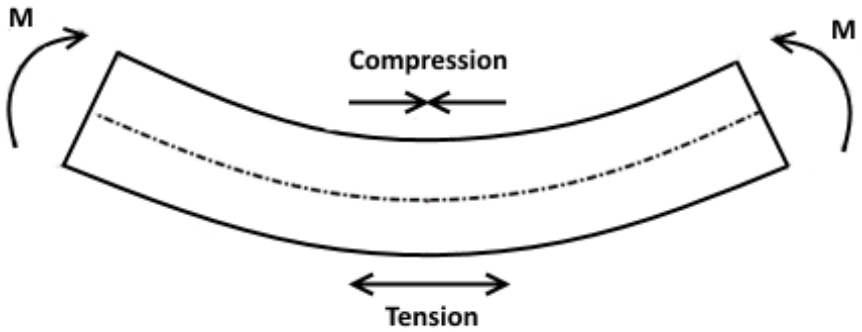

Figure 10. Stress distribution of bending beam.

In Figure 11 the diagram of cyclic loading in tension of commonly used sinusoidal waveform shape is illustrated.

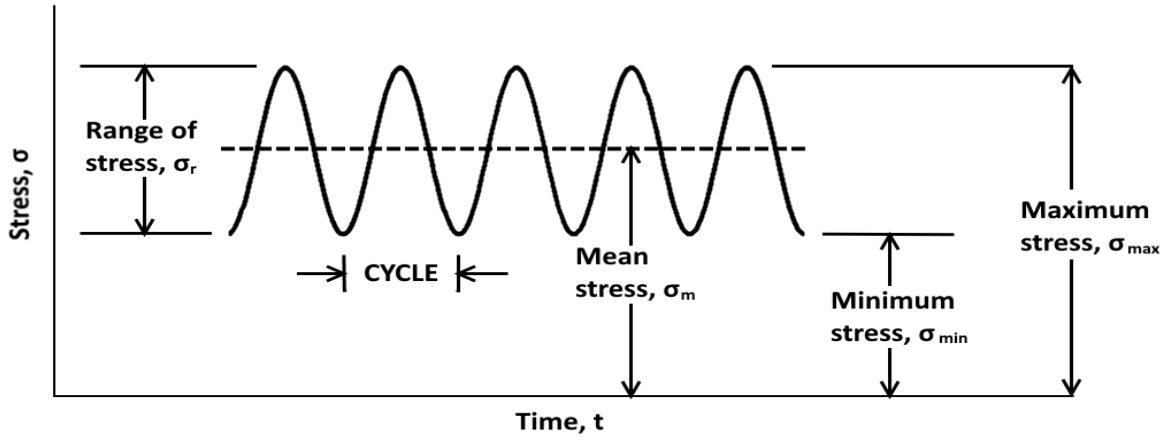

Figure 11. Schematic diagram of symmetric cyclic loading.

In detail, loading force in one cycle may have a different course over time, either it can be constant in time or generate quasi static or dynamic grow over time as is illustrated in Figure 12.

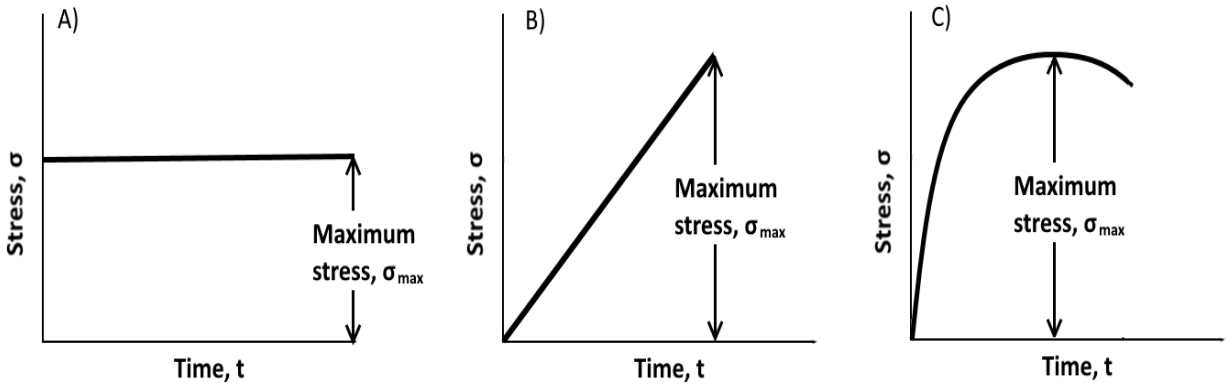

Figure 12. Schematic diagrams of the various loading conditions; A) constant force loading, B) quasi static loading, C) dynamic loading.

For this thesis, two experimental sets each including two compounds with varying concentration of BR and SBR elastomers were prepared. The main purpose was to compare the wear and fracture behaviour to a reference material based on NR. The composition of compounds is shown in Table 1 and a list of used ingredients is given below.

Table 1. Composition of characterized rubber compounds.

	NR	**NR/BR**	**BR**	**NR/SBR**	**SBR**
Natural Rubber	100,0	50	-	50	-
Butadiene Rubber	-	50	100	-	-
Styrene Butadiene Rubber	-	-	-	50	100
Carbon Black	50,0	50,0	50,0	50,0	50,0
Zinc Oxide	3,0	3,0	3,0	3,0	3,0
Stearic Acid	1,0	1,0	1,0	1,0	1,0
Antioxidant	1,5	1,5	1,5	1,5	1,5
Accelerator	2,5	2,5	2,5	2,5	2,5
Sulfur	1,7	1,7	1,7	1,7	1,7

List of used materials

- **Elastomers**
  - ***Natural Rubber***

Standard Malaysian Rubber SMR CV60 from LEE Rubber co.

Dirt [% wt]	0,02
Ash [% wt]	0,50
Nitrogen [% wt]	0,60
PRI Index [min]	60
Mooney viscosity (ML, 1+4, 100°C)	60 +/- 5

  - ***Butadiene Rubber***

Buna CB 24 from Lanxess

Type	Neodymium-BR
Cis 1,4 content [%]	96
Oil	-
Mooney viscosity (ML, 1+4, 100°C)	44

  - ***Styrene Butadiene Rubber***

Buna VSL 4525-0 HM from Lanxess

Type	Solution-SBR
Styrene [%]	25
Vinyl [%]	50
Oil	-
Temperature of glass transition	-22
Mooney viscosity (ML, 1+4, 100°C)	65

- **Fillers**
  - ***Carbon Black***

    STATEX N339
- **Antioxidant**
  - ***IPPD (N-isopropyl-N'-phenyl-p-phenylenediamine)***

    Vulkanox 4010
- **Cure activators**
  - ***Zinc oxide***
  - ***Stearic acid***
- **Cure accelerator**
  - ***CBS (N-cyclohexyl-2-benzothiazolesulfenamide)***

    Vulcacit CZ
- **Curing agent**
  - ***Sulfur***

Before mixing process, all ingredients were weighed within specific tolerances in accordance to ASTM D 3182. All rubber additives were

compounded with raw rubber in two steps. Internal mixer Banbury mixer (Pomini Farrel) was used for the first step and whole process was completed by adding of curing system consisting of an accelerator and sulphur on two roll mill Farrel G-2603 150 x 330 mm. Detailed compounding procedure is given by Table 2.

Table 2. Compounding procedure.

Order	Ingredients	Time [min]	Equipment	Temperature [°C]
1	Elastomer	2	Internal mixer	80
2	Stearic acid + Zinc oxide + IPPD	1		
3	Carbon black	5		
4	CBS	1	Two roll mill	60
5	Sulfur	5		

After mixing, conditioning of the mixed compounds was applied for 24 hours. Vulcanisation characteristics were determined using a rotorless curemeter MDR 3000 Basic (MonTech, Germany) in accordance with ASTM D 5289 at 160 °C for 0.3 hr. and 0.5 arcs with 100 CPM frequency. For vulcanization of test specimens optimum cure time t90 was used (i.e. the time required to reach 90 % of the total state of cure). The test specimens of various shapes had to be moulded at hydraulic press LabEcon 300 by a force 150 kN for each testing method. The prepared specimens were conditioned at ambient temperature for at least 16 hours prior to testing. For tear strength measurements in tension, direction of rolling was parallel to the applied tensile force.

4.1 Measurement of mechanical properties of vulcanizates

In order to determine basic mechanical properties of tested rubber materials, measurements of hardness, quasi-static tensile test and dynamic mechanical analysis were performed.

4.1.1 Hardness Shore A

For fundamental characterization of rubber hardness properties Shore durometer was used. For rubber vulcanizates Shore A method according to ISO 7619 is the most appropriate. The principle of determination Shore hardness is based on measurement of penetration resistance of pin into the material.

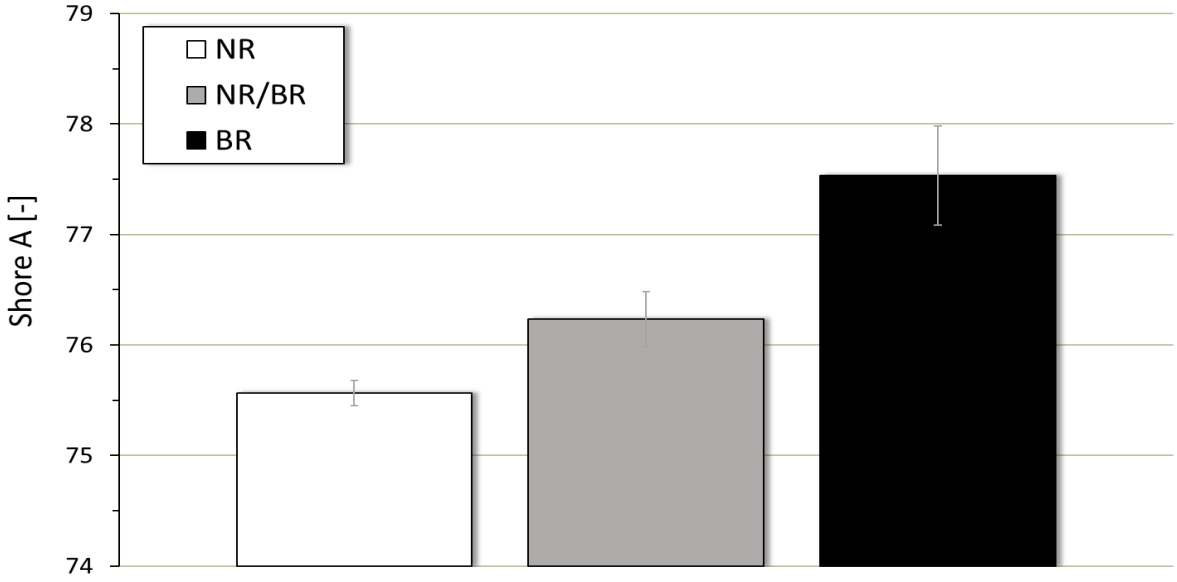

Figure 13. Results of Shore A hardness of NR, NR/BR and BR.

For both sets of materials, it is visible that addition of BR or SBR increased value of Shore A hardness which is characteristic for rising level of material elasticity.

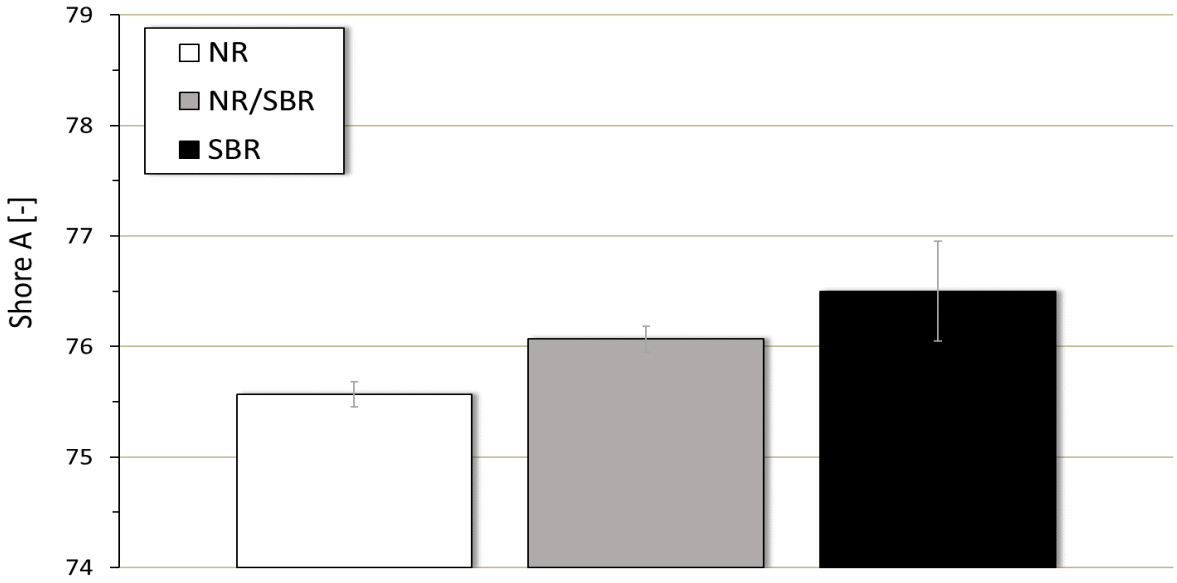

Figure 14. Results of Shore A hardness of NR, NR/SBR and SBR.

4.1.2 Tensile test

Displacement controlled tensile test in accordance with ISO 37 using dumbbell specimen type B was used as another method for characterization of mechanical properties. Tensile test was conducted at room temperature at a constant displacement rate of 500 $mm.min^{-1}$. The tensile strength, elongation and modulus were plotted as functions of the changes of mechanical properties in dependence on percentage representation of each elastomer in rubber compound.

From results, which are represented in Figures 15 it is visible that strength and elongation in tension reached the highest value for reference material prepared only based on NR. These good tensile properties are given by ability to strain induced crystallization. With increasing content of elastomers that do not strain crystallize such as BR and SBR strength and elongation in tension were decreased.

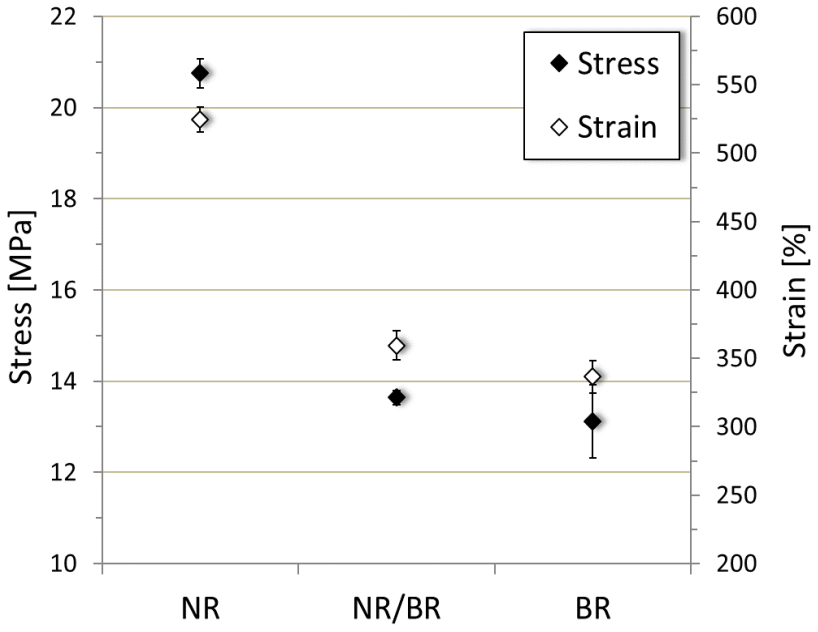

Figure 15. Results of stress and strain of NR, NR/BR and BR.

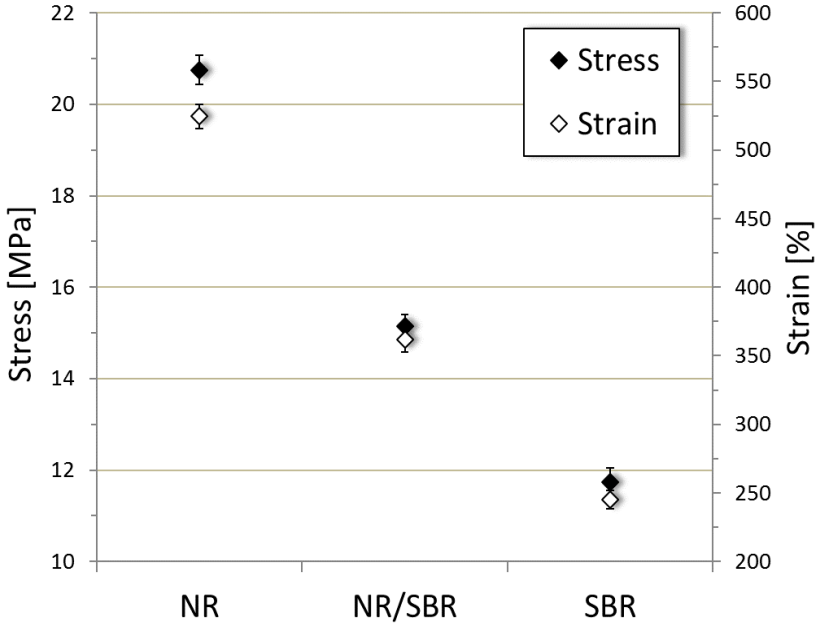

Figure 16. Results of stress and strain of NR, NR/SBR and SBR.

Figures 17 and 18 depict values of stress that were measured at 50, 100 and 200 % of elongation. From these results it is evident that NR shows the most pliable behaviour for elongation up to 100 % in comparison with other tested materials and with SBR based material also for 200 % elongation. SBR containing styrene sections in polymeric chain are characterized by increased mechanical stiffness. For materials with presence of BR the value of stress necessary to elongate to 200 % decreases in comparison with NR. This effect is most probably caused by beginning of predomination of strain induced crystallization of NR.

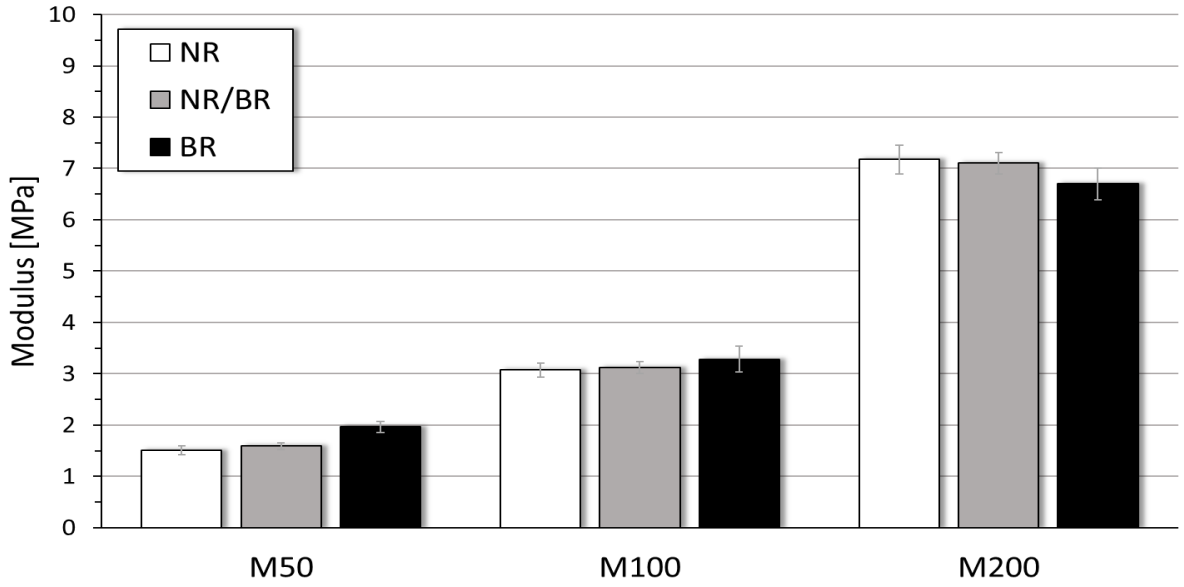

Figure 17. Results of stress necessary to elongation of 50, 100 and 200 % of NR, NR/BR and BR.

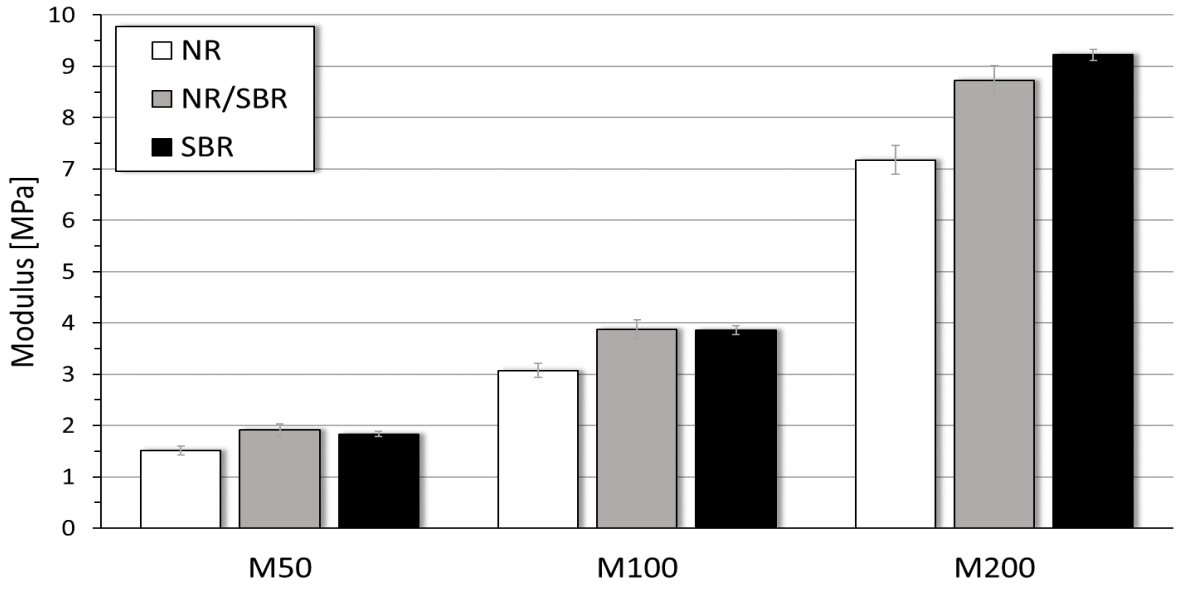

Figure 18. Results of stress necessary to elongation of 50, 100 and 200 % of NR, NR/SBR and SBR.

4.1.3 Dynamic mechanical analysis

Dynamic mechanical analysis (DMA) was used to examine effect of temperature on viscoelastic properties of rubber compounds. Using DMA progress of Tan δ depending on temperature and material formulation was determined. Tan delta which is given as ratio of loss to the storage modulus indicates degree of dissipation of energy. Increase in Tan delta indicates that material has bigger energy dissipation potential thus material exhibits higher degree of damping. Measurement was performed in shear mode by DMA (Mettler Toledo, Switzerland) according to ISO 4664. Damping of rubber materials was determined in the temperature range, which corresponded to the conditions of the measurement of fracture behaviour by tensile impact test.

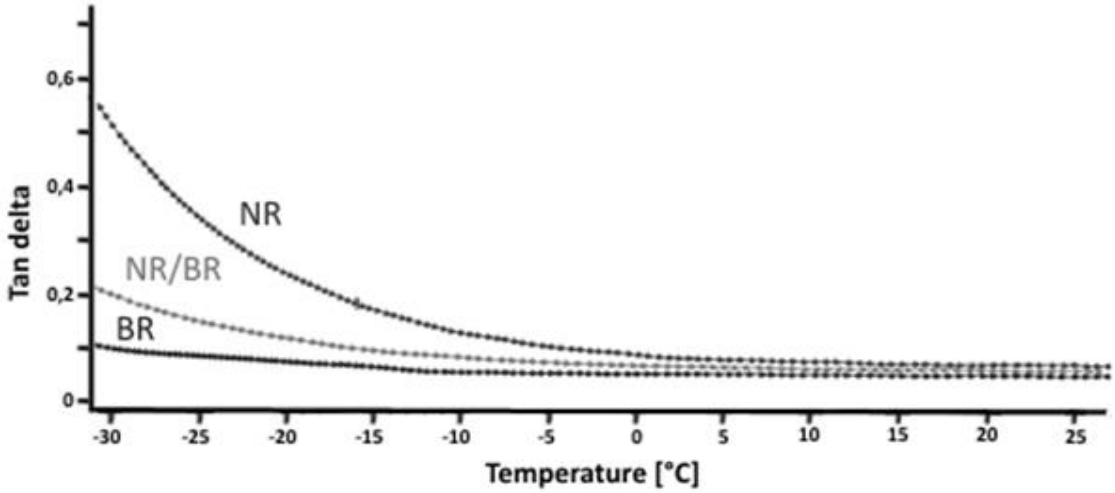

Figure 19. Dependence of Tan delta vs. temperature of NR, NR/BR and BR.

The progress of Tan delta signal displayed in Figure 19 shows that rubber based only on NR exhibits the highest degree of damping at temperatures below freezing point for set of materials with BR addition. Ability to damping decreases with rising concentration of BR.

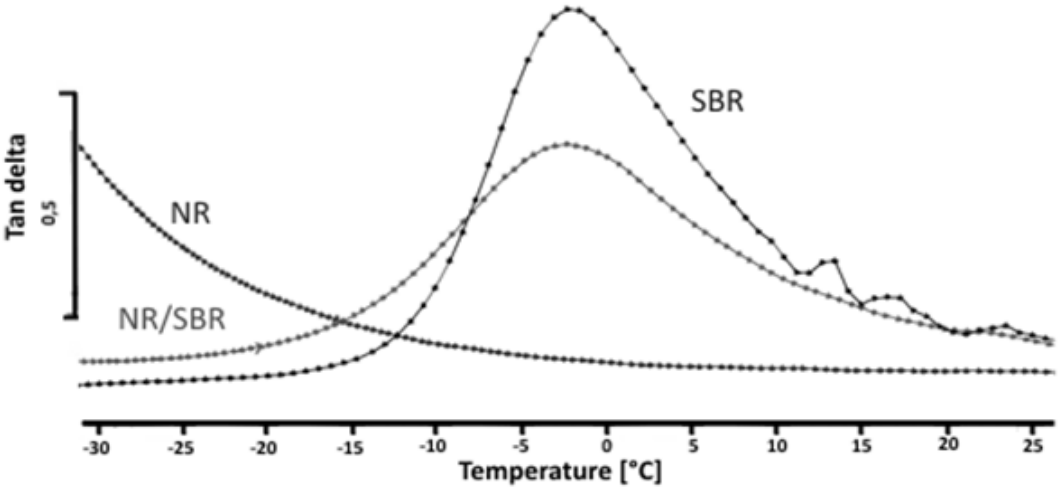

Figure 20. Dependence of Tan delta vs. temperature of NR, NR/SBR and SBR.

The Figure 20 illustrates dependence of Tan delta signal on temperature for materials containing SBR. From these results it is visible that Tan delta signal of NR/SBR and SBR exhibited peaks which indicated value of *Tg* where rubber changes from glassy state when material is brittle to rubbery state.

4.2 Determination of wear and fracture properties of vulcanizates

In order to describe wear and fracture behaviour a few mechanical methods of testing both dynamical and cyclic were performed. Using these tests, it is possible to characterize influence of type and rate of loading on fracture behaviour of each used elastomer. Interpretation of results is focused on definition of influence of commonly used synthetic elastomers on durability at each stage of rubber product failure.

4.2.1 Determination the wear resistance behaviour using the abrasion resistance test

The wear properties were investigated by abrasion resistance test represented by moving the tested specimen across the surface of abrasive sheet mounted to revolving drum as this principle is well known and standardized. This testing method could fundamentally simulate process of tire sliding on the road surface when a rubber specimen is sliding on sandpaper with hard rough surface. Thus tensile stress is developed in the region of rubber and asperity contact. Wear process is represented by two different phenomena. If tensile stress is high enough, nucleation of crack appears. Which then continues to propagation of the crack resulting in detachment of rubber particles. Normal length of abrasion path used for standard method according to ASTM D5963 is 40 meters. For deeper determination of wear resistance, the abrasion length was set to the 200 meters. Dependence of weight loss on the length of abrasion path is given as a result of this test.

As it is seen in Figure 21 the weight loss was the lowest for pure BR throughout the test period. It is a feature of a good resistance against crack nucleation. This property is due to low amount of shear stress generated in contact area with asperities thanks to low loss modulus of BR at testing conditions. Results also indicate that added content of BR in compound with NR improves resistance to abrasion by more than a half.

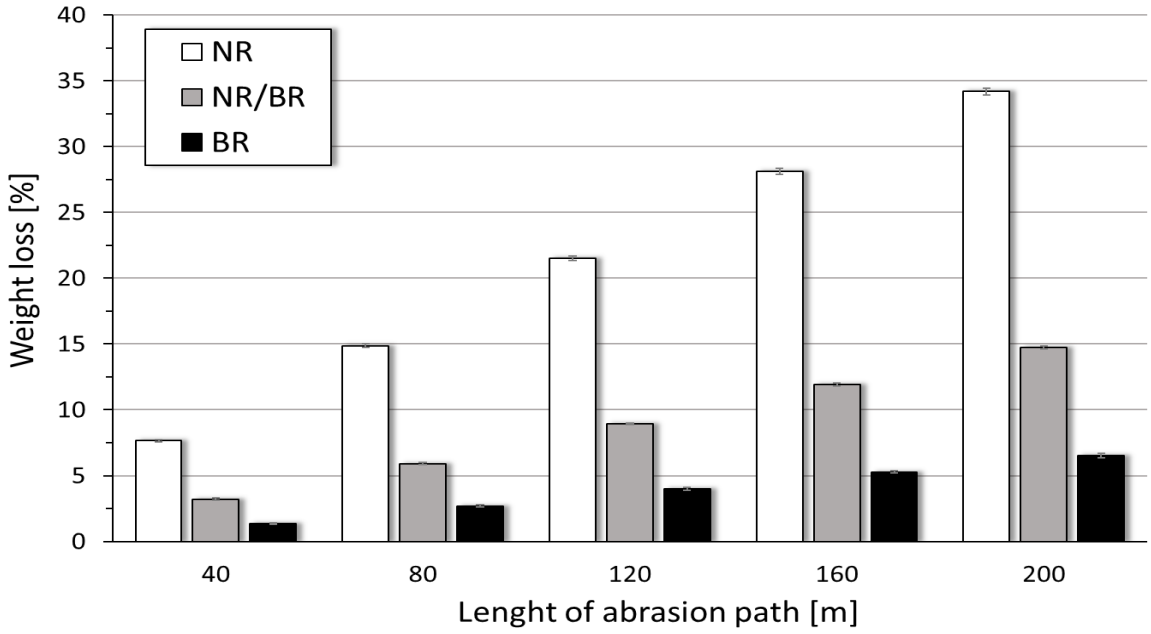

Figure 21. Results of abrasion test of NR, NR/BR and BR.

Figure 22 shows results of materials with SBR content. In comparison with NR values, slight decline of wear resistance is visible. It is caused by higher amount of friction between rubber and abrasive surface of SBR due to viscoelastic behaviour. Increment of friction results in stronger shear stresses and higher temperatures in contact area, thus higher rate of crack initiation. The 50/50 NR/SBR compound possess the wear resistance which could be caused by bad cohesion of NR and SBR segments in matrix.

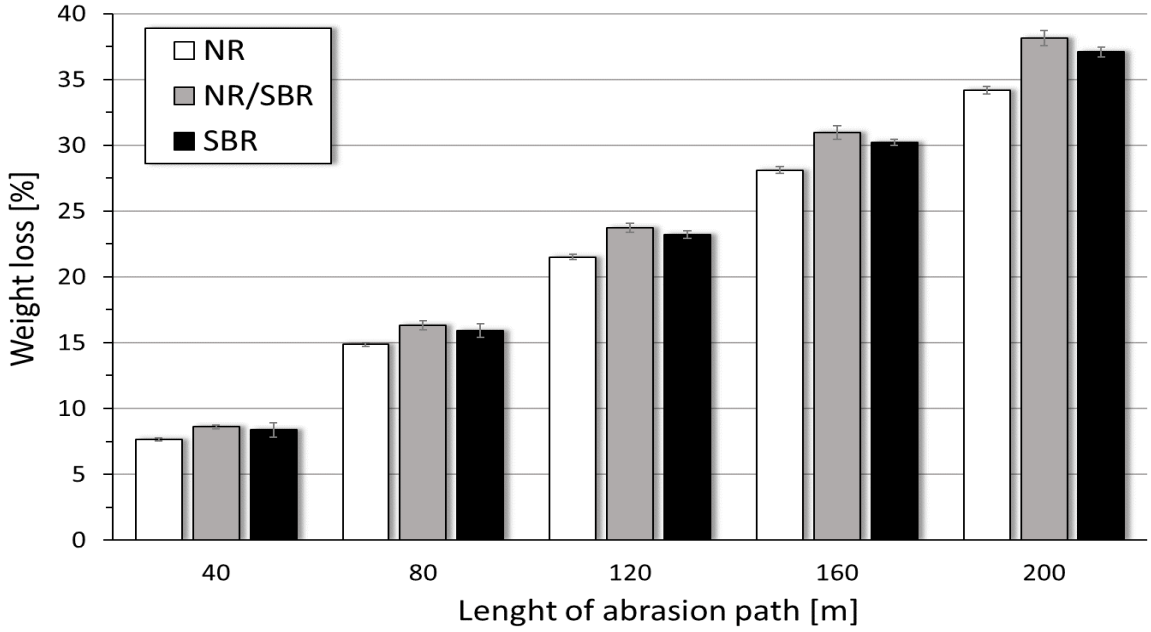

Figure 22. Results of abrasion test of NR, NR/SBR and SBR.

4.2.2 Determination of impact resistance by free falling dart method

For characterization of resistance against penetration of unnotched specimen at high rate of deformation free falling dart method which is described by ISO 6603-2 was used. The principle of this method consists in penetration of clamped test specimen by a lubricated striker at a nominally uniform velocity. The force – extension diagram could be divided into two parts which determine fracture behaviour of unnotched specimen under impact. Cracking energy E_{cr} corresponds to area under force – deformation diagram bounded by the origin to F_{cr} and provides information about resistance to crack initiation. Energy necessary to penetration of cracked specimen is described by area between F_{cr} and maximal penetrant force F_{pen} and characterizes resistance to crack propagation.

Impact resistance test was performed by impact tester Fractovis 6789 (CEAST, Italy) with standard striker velocity 4,4 m/s. Characteristic fracture values as the energy in the cracking point where any cracks that can be observed by the naked eye and the energy that is needed to supply to penetrate striker through the entire thickness were defined for each material. Five standard test specimens with dimensions 60 x 60 x 2 mm were measured for each material.

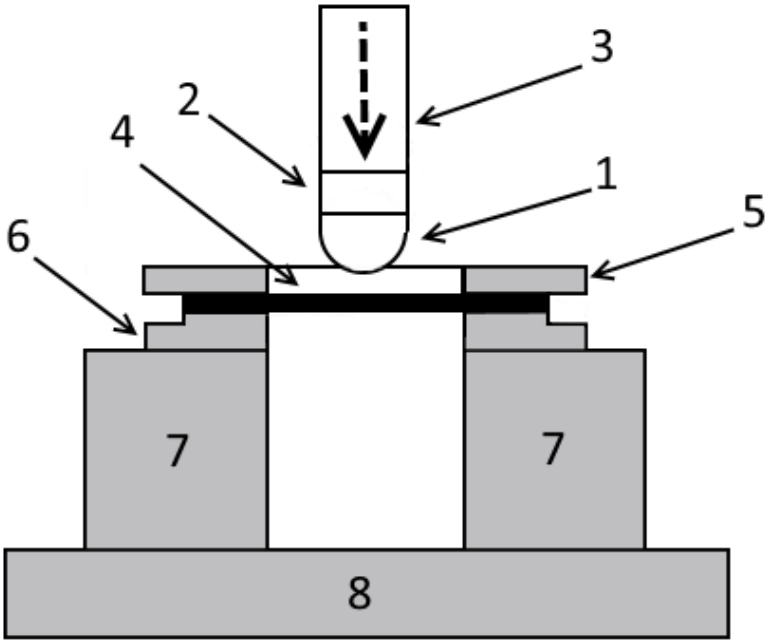

Figure 23. Functional principle and visualization of free falling dart equipment, where: 1 – hemispherical striker tip; 2 – load cell; 3 – shaft; 4 – test specimen; 5 – clamping ring; 6 – test specimen support; 7 – base; 8 – acoustical isolation.

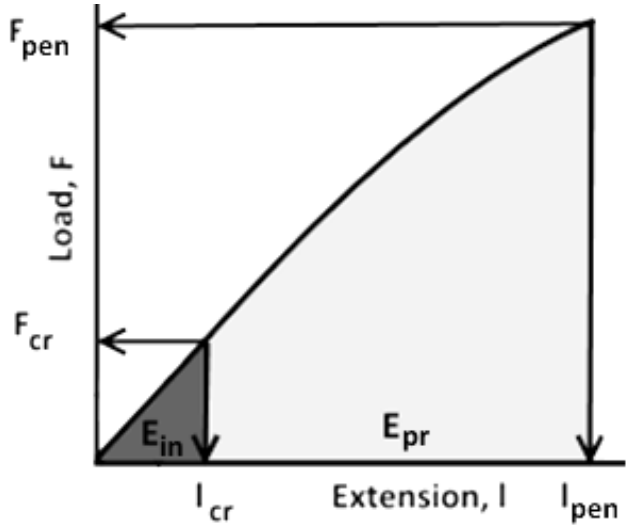

Figure 24. Schematic diagram of load – extension progress obtained by free falling dart test.

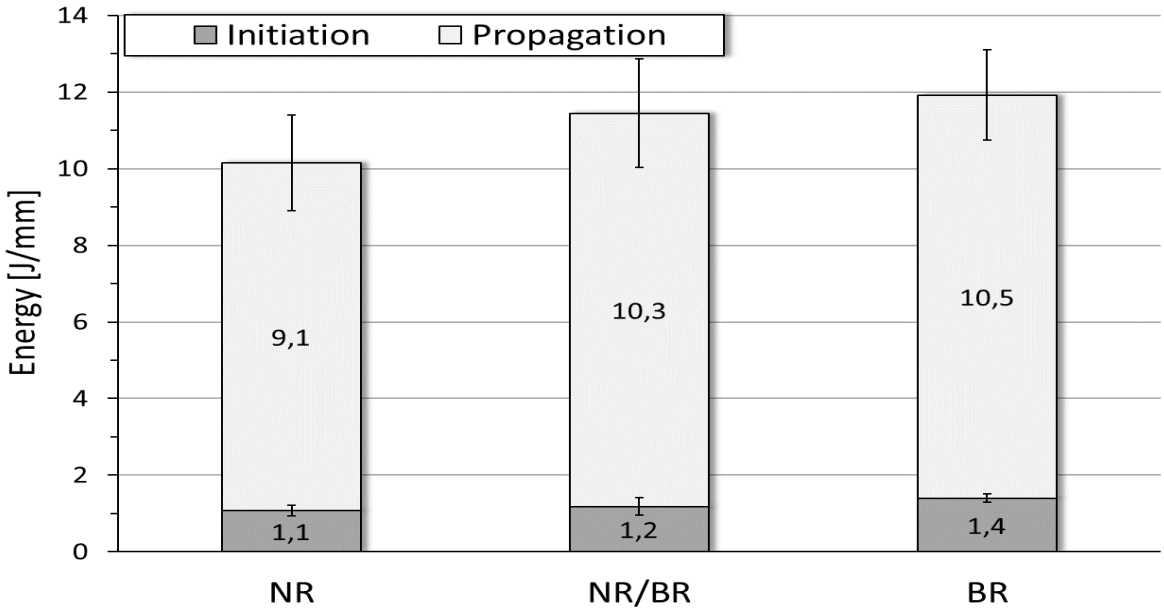

Figure 25. Summary of energy necessary to initiation and propagation of cracks in unnoched specimens of NR, NR/BR and BR.

Figure 25 shows the energy necessary to penetration of specimen which is divided into two stages representing crack initiation and propagation. From these results it is visible that presence of BR in compounds improves crack initiation resistance and also resistance to penetration. Furthermore, it is obvious that value of energy required to break grows with rising concentration of BR.

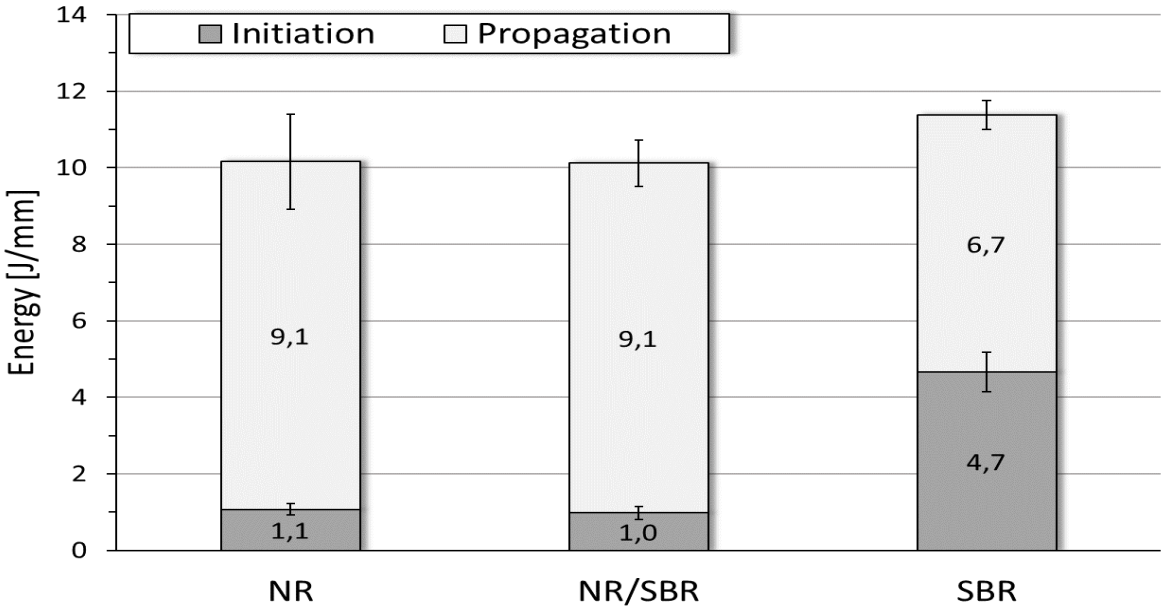

Figure 26. Summary of energy necessary to initiation and propagation of cracks in unnoched specimens of NR, NR/SBR and SBR.

As can be seen in Figure 26 material based on NR and its compound with SBR exhibits similar fracture properties as NR/BR compound. Material consisting solely from SBR exhibited the highest resistance to formation of crack by striker at high rate of deformation. Value of energy necessary to crack formation was approximately 4,5 times higher than for other materials. This could be caused by both presence of styrene parts in molecules of SBR which carry strength and fact that energy necessary to crack propagation is lower in comparison with other materials due to brittle behaviour of SBR in this phase. Furthermore, the increased mechanical modulus of SBR was reflected by higher value of energy necessary to penetrate the sample thickness completely.

In conclusion, both commonly used synthetic rubbers have higher degree of resistance against penetration compared to NR.

4.2.3 Determination the crack resistance behaviour using instrumented notched tensile impact test

The instrumented notched tensile-impact test is an extension of the conventional tensile-impact test according to ISO 8256 generally used determine toughness properties of polymeric materials. In this case application of the instrumented Charpy impact test is not possible because of the specimen thickness and low material stiffness. [62] This method should be applied especially within testing of polymeric sheets and elastomers. [63]

The determination of crack resistance was performed by pendulum device Resil Impactor Junior 25 (CEAST, Italy) according to ISO 13802 with impact energy 7,5 J and falling angle 150°. Double-edge-notched tension (DENT) specimens were used for testing.

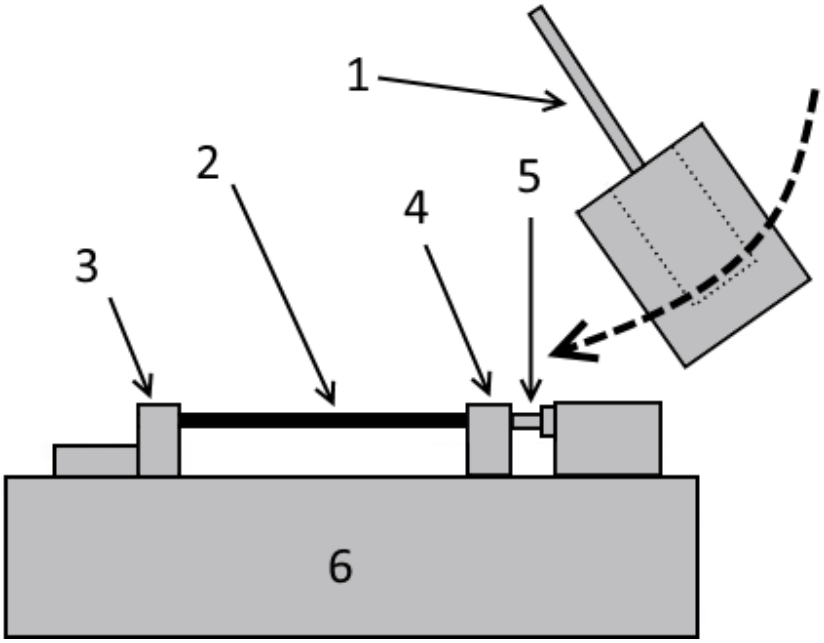

Figure 27. Functional principle and visualization of tensile impact test equipment, where: 1 – pendulum hammer; 2 – test specimen; 3 – crosshead; 4 – stationary clamp; 5 – base

Ten test specimens were analysed for each material. DAS4WIN software that displays force – extension diagram which schematic shape typical for elastomer is depicted in Figure 28 was used for analysis data. Area under force – extension curve is divided into two parts: A_{max} determines energy up to maximum load which characterize resistance to crack propagation; A_p represents crack propagation energy. The area under A_p gives information about ratio between stable and unstable crack propagation. When the area of A_p is small, the process of unstable crack propagation when crack spreads without supplying any additional energy is dominant.

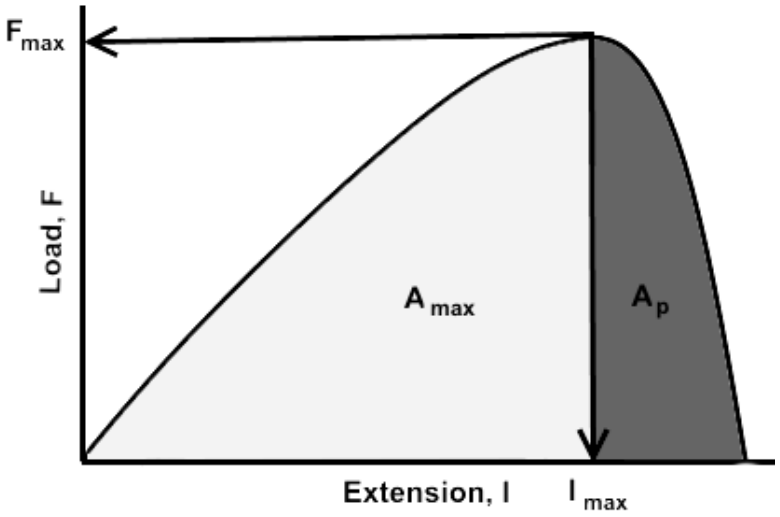

Figure 28. Schematic diagram of load – extension progress obtained by impact tensile test.

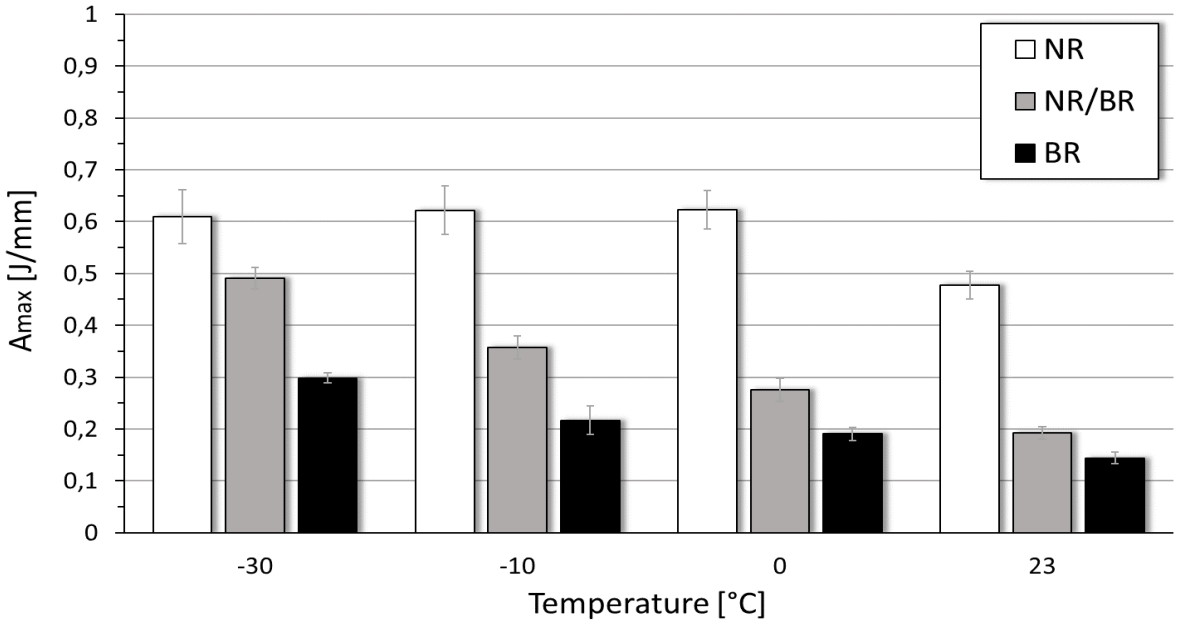

Figure 29 Results of energy associated with resistance crack growth of NR, NR/BR and BR.

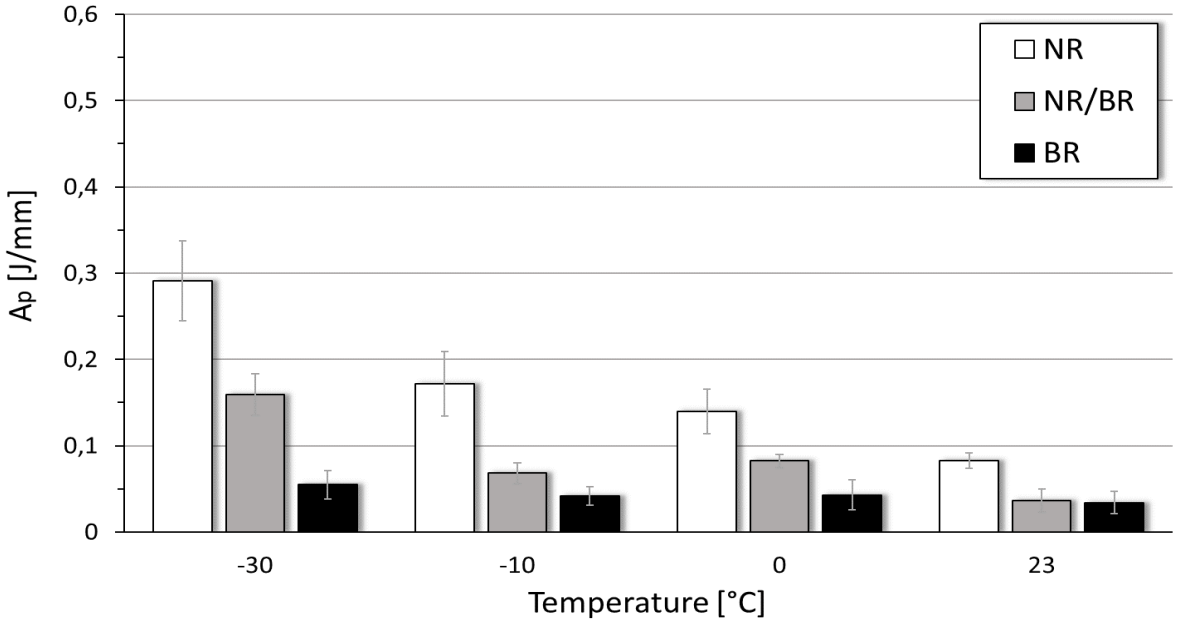

Figure 30. Results of energy associated with crack growth of NR, NR/BR and BR.

Energy necessary to growth of created notches decreases with rising content of BR, whereas material based only by BR exhibits the lowest level of crack propagation resistance. Furthermore, the effect of temperature shows that energy required for crack propagation increases with decreasing temperature. This trend is caused by increasing degree of material stiffness and necessity to reach higher energy needed to crack propagation. Second part of area under force – extension curve indicates how much energy is necessary to add to spread crack leading to rupture. Results indicate that energy required to crack propagation is higher for NR than NR/BR and BR material, thus NR exhibits the highest ratio of stable

crack propagation. On the other hand, crack in BR spreads unstably at lower energy values. The decline of temperature leads to improvement of fracture resistance.

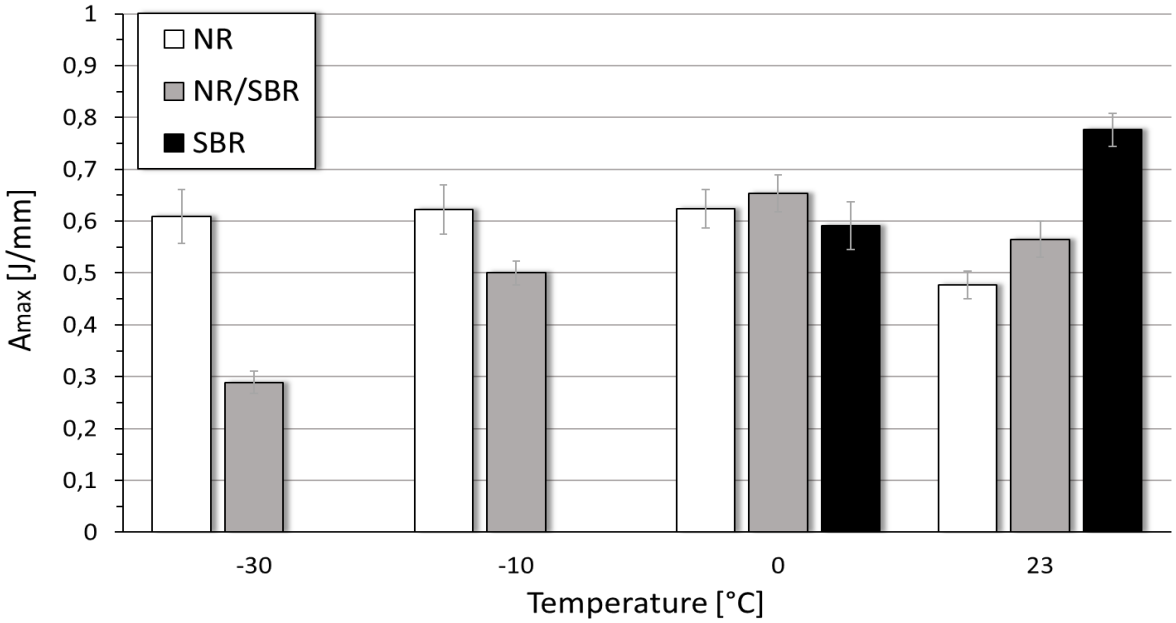

Figure 31. Results of energy associated with resistance to crack growth of NR, NR/SBR and SBR.

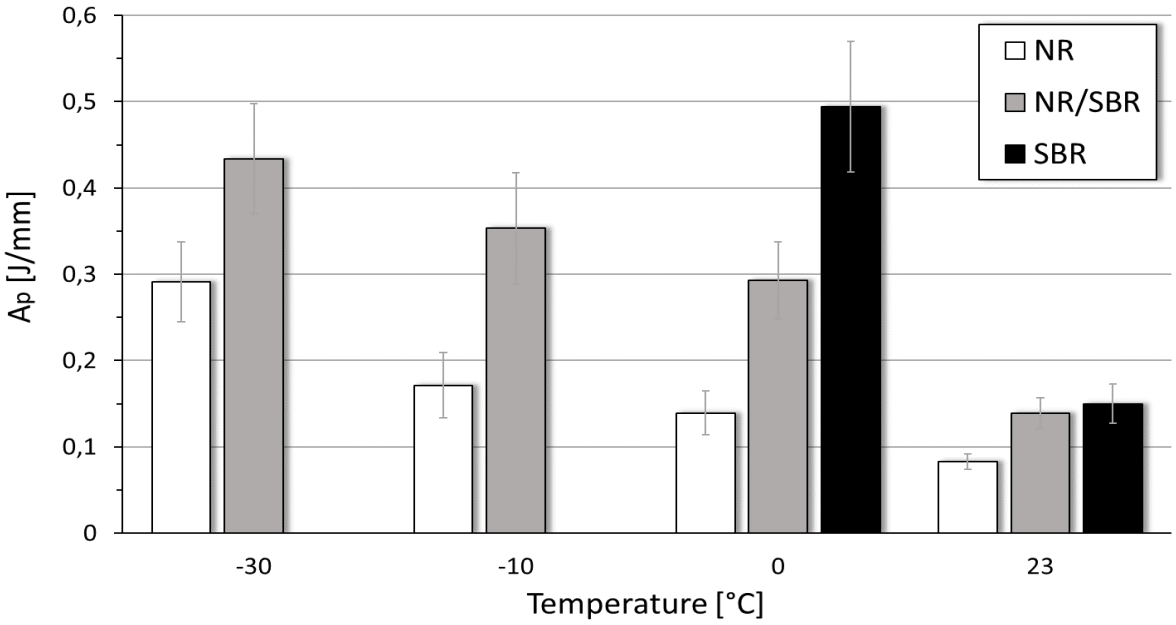

Figure 32. Results of energy associated with crack growth of NR, NR/SBR and SBR.

From results which are shown in Figure 32 it is evident that presence of SBR improves level of crack propagation resistance but only for temperature to the freezing point. With temperature approaching to the temperature of glass transition decline of energy absorption is visible. The energy absorption can be

supplied before rupture occurs. For NR/SBR better resistance to crack propagation at 0 °C and for temperatures under zero together with huge decline of fracture properties is visible. Also effect of decreasing temperature on increase of energy *Ap* is visible. For temperatures under glass transition material formed by pure SBR exhibits brittle behaviour therefore it was not possible to complete characterization due to fracture in a different part of specimen.

Materials exhibiting elastic behaviour are able to absorb a huge amount of energy and deform without occurring fracture, this ability is called impact toughness. For DENT test specimens was calculated on basis of knowledge A_{max} energy by Equation 19 according to Grellmann and Reincke [64].

$$J = \frac{\eta A_{max}}{d(l-a)} \tag{19}$$

$$\eta = -0{,}06 + 5{,}99\left(\frac{a}{l}\right) - 7{,}42\left(\frac{a}{l}\right)^2 + 3{,}29\left(\frac{a}{l}\right)^3 \tag{20}$$

where A_{max} is energy up to maximum load, d is thickness of specimen, l is length of specimen and a is total crack length.

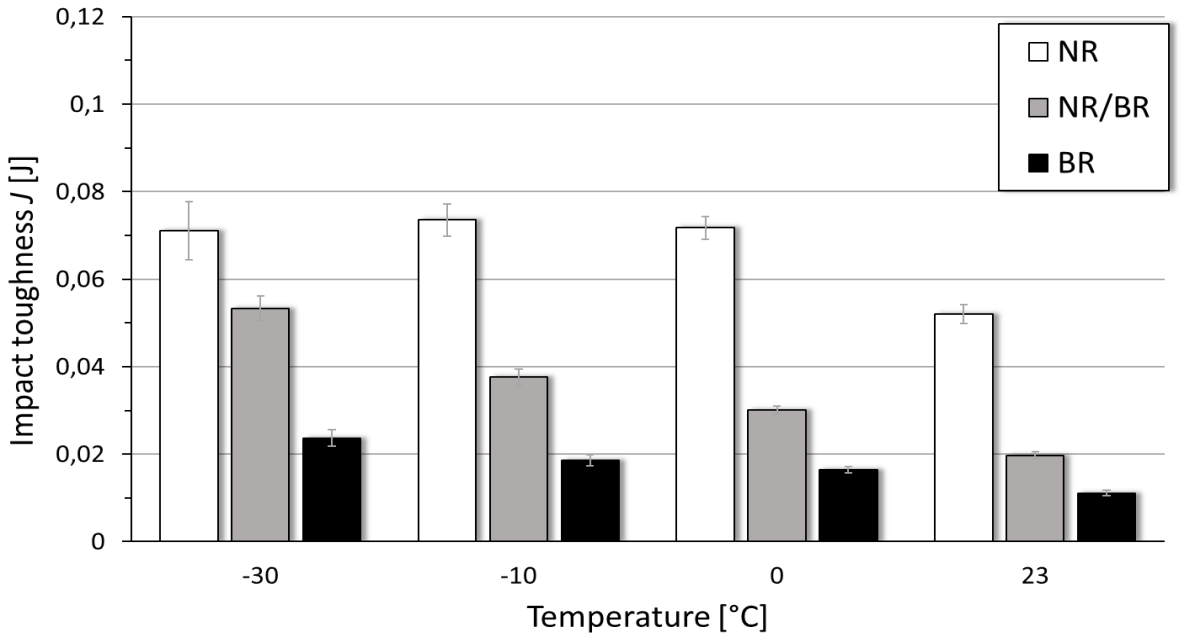

Figure 33. Results of impact toughness of NR, NR/BR and BR.

In general, NR has good impact toughness as can be seen in comparison with BR which exhibits the lowest impact toughness. Compound of NR and BR reaches values between NR and BR. Temperature has an influence on rate of impact toughness value. With decreasing temperature, the ability to absorb energy without rupture increases. Under zero degree of Celsius NR exhibits only slight improvement.

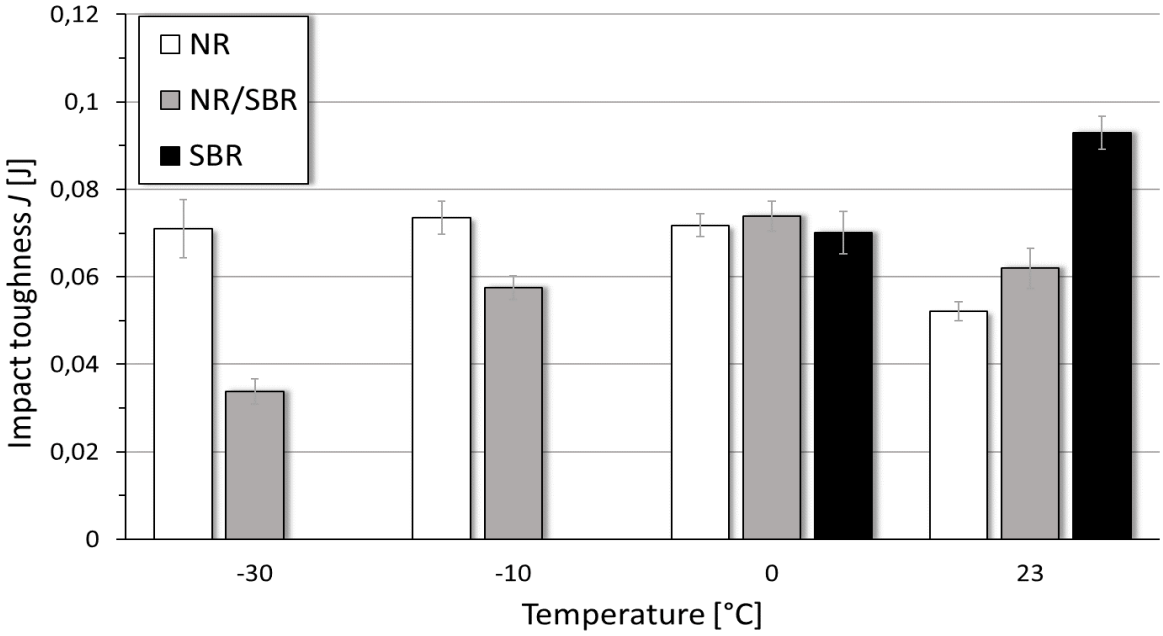

Figure 34. Results of impact toughness of NR, NR/SBR and SBR.

SBR and their compound with NR achieve better impact toughness at room temperature than NR in comparison with BR. But ability to absorb energy rapidly decreases with decreasing temperature. This phenomenon is given by reaching the temperature of glass transition of SBR at higher temperature than NR. At temperature near the glass transition material becomes more brittle and loses its ability to absorb energy and deforms without rupturing.

From results of crack resistance determination under impact in tension influence of viscoelasticity is evident. BR is a material with Tan delta peak occurring at temperature far below freezing. Due to this property it can be assumed that energy necessary to crack propagation will be lower for BR and on the other hand SBR should exhibit the best resistance to crack grow which have the temperature of glass transition slightly under zero degree of Celsius. Both assumptions were confirmed experimentally using DMA analysis.

4.2.4 Crack propagation resistance under cyclic loading condition

Fatigue crack growth properties of vulcanizates were measured using a Tear and Fatigue Analyser (Coesfeld, Germany) which is an instrument allowing a quantitative analysis of fatigue crack growth processes on test specimens using varied loading waveform, within frequency range 0,1 - 50 Hz. The device is equipped by CCD monochrome camera and image processing software that is integrated in this equipment to measure crack length and crack contour of sample. Evaluation of fracture characteristics is in accordance with Rivlin and Thomas theory.

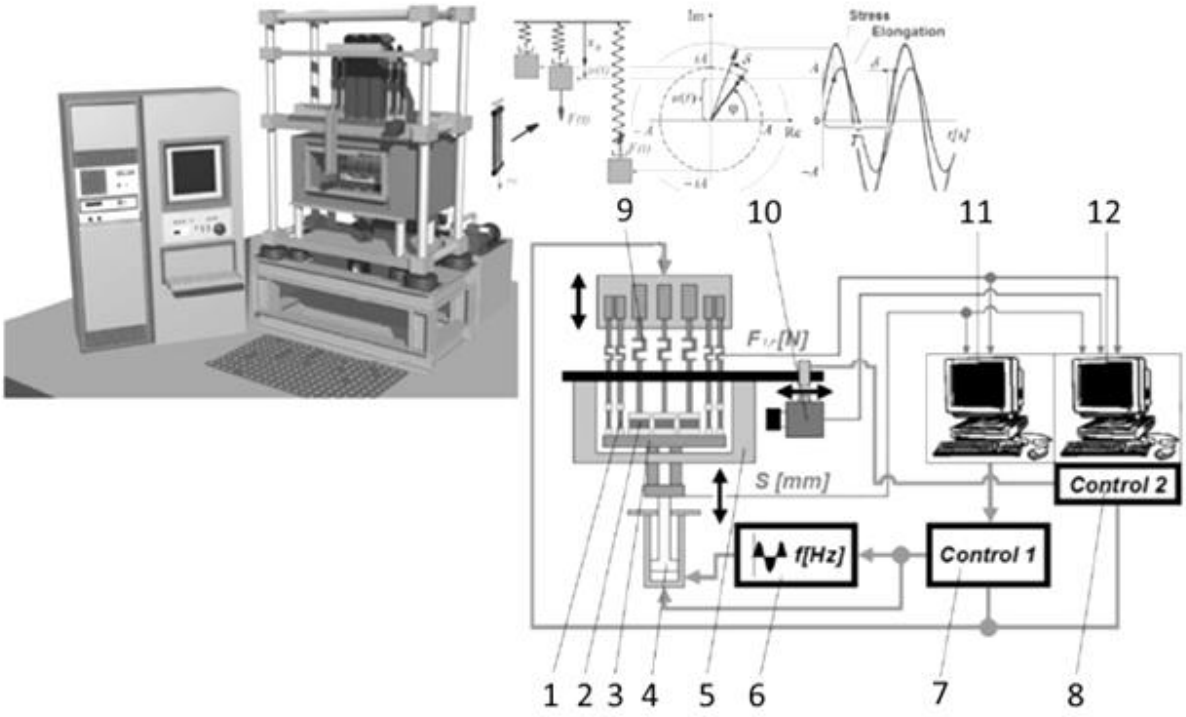

Figure 35. Schematic and functional diagram of the tear analyzer: 1 – tensile test piece; 2 – pure-shear test piece; 3 – traverse; 4 – hydropulzer; 5 – isolated chamber; 6 – frequency generator; 7 – control unit 1; 8 – control unit 2; 9 – load cells; 10 – CCD monochrome camera; 11 – PC1; 12 – PC2.

Fatigue crack growth measurements under sinusoidal loading with frequency 10 Hz for strains from 10 to 20 % were performed for vulcanizates. For materials containing BR were chosen deformation up to 15 % due to high velocities of FGC at higher values of strain. For each strain, three pure shear specimens were analysed. Results analysed with TFA are represented by double logarithmic plot of tearing energy, *T* versus crack growth rate (*da/dn*) that is shown in Figures 36 and 37. From Figure 36 representing comparison of crack growth behaviour of NR, BR and their compound it is visible that vulcanizates based on NR exhibit the lowest crack growth rate at strain of 15 %. That indicates NR having higher fatigue crack growth resistance compared to BR and compound of NR with BR. Furthermore, NR has a lower crack growth rate at higher values of tearing energy than BR.

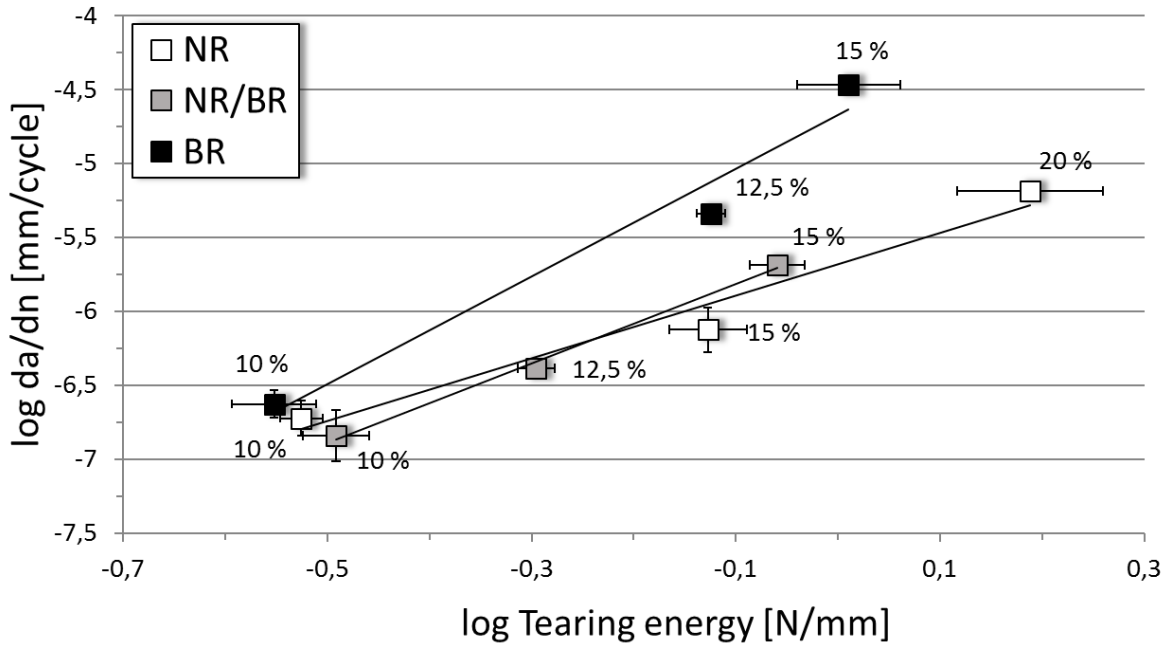

Figure 36. Dependence of fatigue crack growth rate vs. tearing energy of NR, NR/BR and BR.

Influence of SBR presence is seen in Figure 37 where results of NR, NR/SBR and SBR are shown. These measured data indicate that SBR elastomer exhibits lower resistance to crack growth in comparison with NR and NR/SBR which are characterized by using the same conditions. However, NR exhibits slightly better resistance to crack growth at higher level of strain than SBR and compound of NR and SBR.

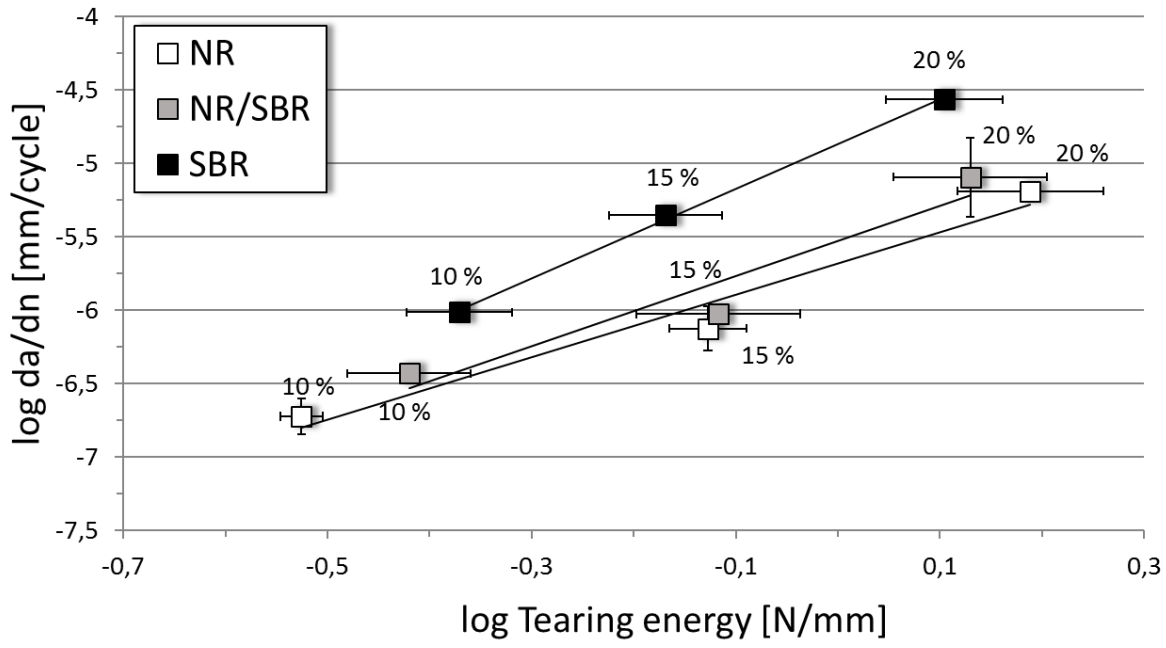

Figure 37. Dependence of fatigue crack growth rate vs. tearing energy of NR, NR/SBR and SBR.

4.2.5 Determination of crack growth resistance at rubber specimen which is cut by a sharp object

For characterization of resistance against crack propagation at pre-stressed rubber test specimen which is cut by sharp object newly developed device made in cooperation with Co. PRL Polymer Research Lab., s.r.o. (Zlín, Czech Republic) was used. The system uses the theoretical background and cutting method of Lake & Yeoh. [64] Principle of measurement is based on application of fully instrumented and electrically driven testing equipment, which is able to apply various loading force. Visualization of testing equipment is illustrated in Figure 38. The test specimen (6) fixed in a clamping system (7) and (8) is pre-stressed due to actuator of the axis Y (1) by given force which is controlled by load cell (3) in a strain direction Y. The actuator (2) provides movement of tip of razor blade (5) in an orthogonal direction to main loading stress applied to specimen. The process of cutting by razor blade tip is used as simulation of crack initiation by sharp object. Movement of razor blade through test specimen is provided by cutting force which is observed and controlled by load cell (4) throughout duration of analysis. The fracture mechanics phenomena were described on pure-shear test specimens. Measured data were used for calculation of the characteristic fracture values such as tearing energy *T*, which is responsible for rubber test specimen tearing process according to Rivlin & Thomas energy criterion. [65]

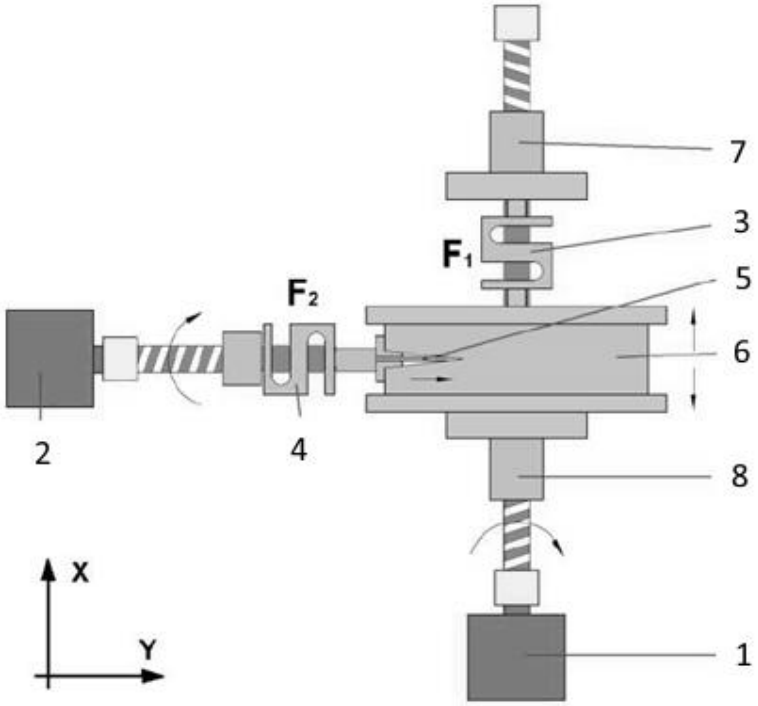

Figure 38. Functional principle and visualization of testing equipment for experimental characterization of crack initiation, where: 1 – actuator of the axis Y; 2 – actuator of the axis X; 3 – loading cell of the axis X; 4 – loading cell of the axis Y; 5 – razor blade; 6 – test specimen; 7 – upper clamping system of test specimen; 8 – bottom clamping system of test specimen. [2]

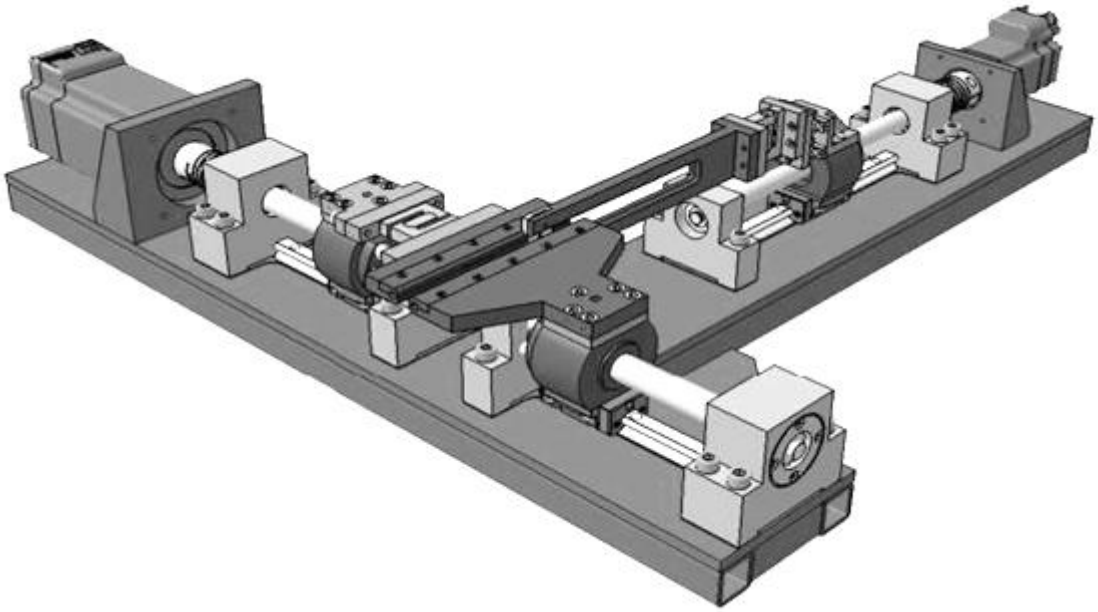

Figure 39. 3D visualization of device.

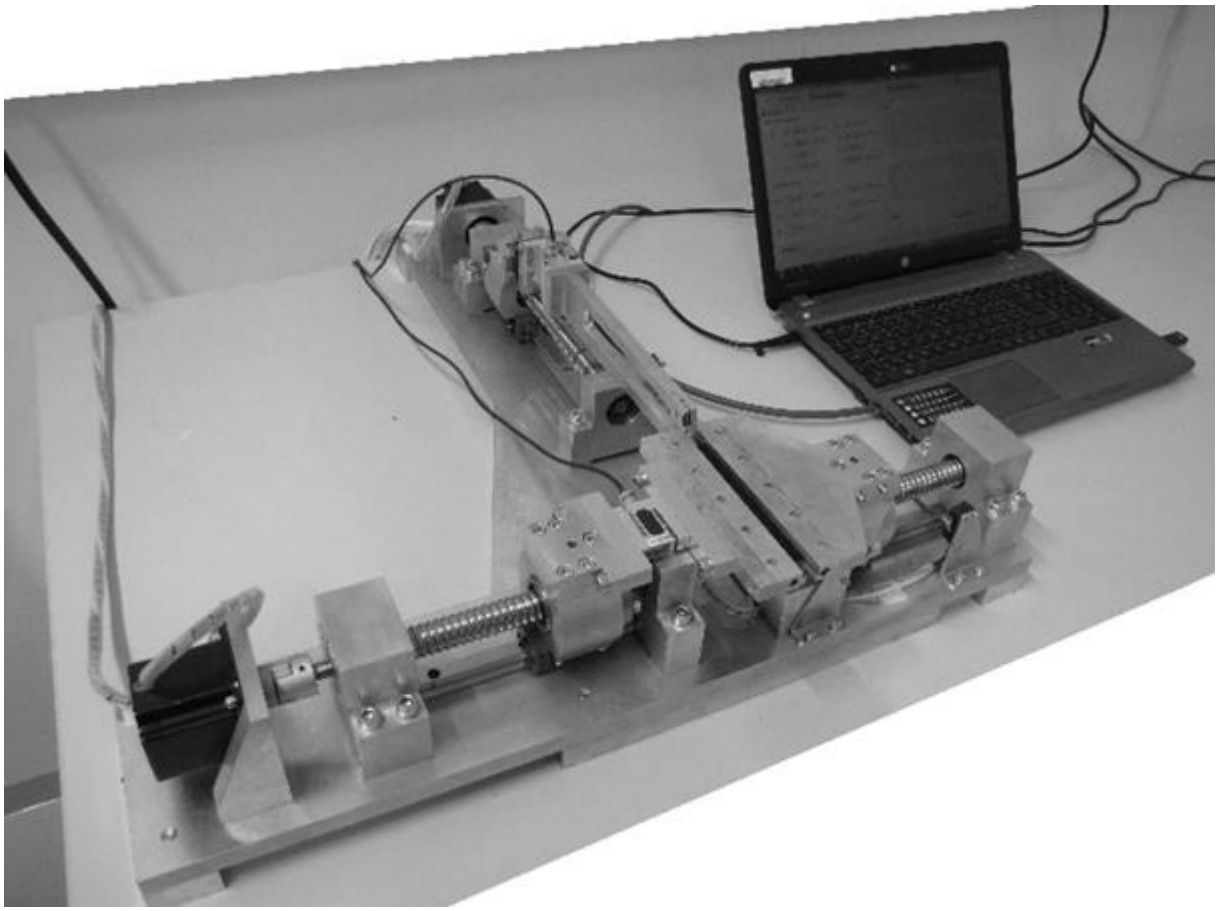

Figure 40. Real visualization of the device.

Influence of applied amount of cutting velocity, v_x; pre-force, F_y; and thickness of razor blade, d_b on change of tearing energy were evaluated from obtained data. Testing conditions, which were applied, are provided in Table 3.

Table 3. List of applied testing conditions used for crack propagation resistance.

Designation	**Cutting velocity, v_x [mm/min]**	**Pre-force of test specimen, F_y [N]**	**Thickness of razor blade, d_b [mm]**
XX_25_50_4	25	50	0,4
XX_25_50_1	25	50	0,1
XX_100_50_4	100	50	0,4
XX_100_50_1	100	50	0,1
XX_25_100_4	25	100	0,4
XX_25_100_1	25	100	0,1
XX_100_100_4	100	100	0,4
XX_100_100_1	100	100	0,1

XX – BR, NR/BR, NR, NR/SBR, SBR

Three standard pure-shear geometry specimens with length to width ratio of 8:1 were analysed for each pre-set condition and average values are plotted as results.

The designation of each test specimen set is given by the code:

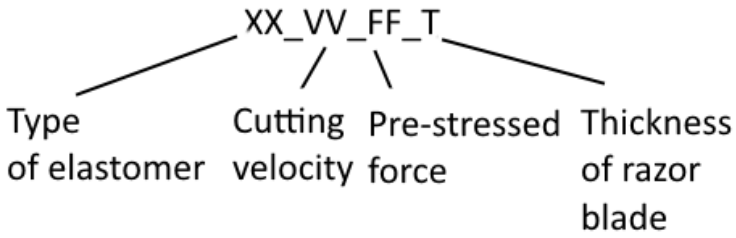

From graphs illustrating dependence of tearing energy increment ΔT that has been calculated by Equation 11 on crack length durability of material which is represented by rate of strain energy necessary to crack propagation can be deduced. Moreover, the ratio between stable and unstable crack propagation and value of critical tearing energy increment ΔT_{cr} causing rupture of specimen can be determined.

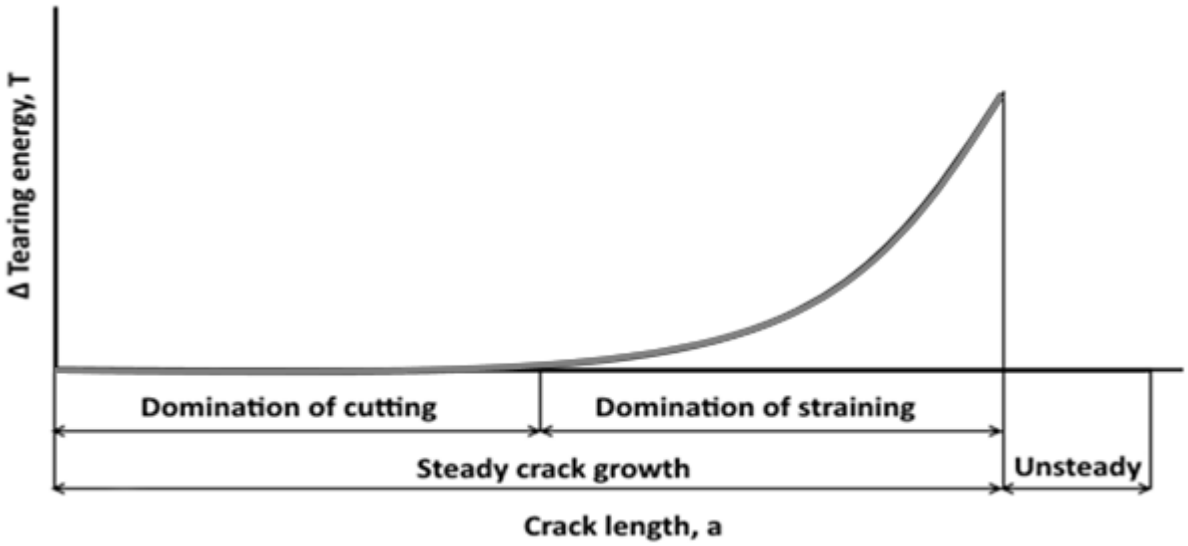

Figure 41. Schematic graph of dependence of tearing energy increment vs. crack length.

A typical curve illustrating dependence of increment of tearing energy ΔT caused by strain force on crack length is shown in Figure 41. Course of this curve can be divided into three parts. In the first part, contribution of tearing energy T is insignificant and close to zero, thus the propagation of crack is primarily caused by cutting. In second part growing contribution of tear energy caused by strain force is visible. This trend is due to the fact that velocity of crack growth becomes higher than velocity of razor blade movement. In this part increment of tearing energy increases. Region of steady state crack propagation is topped by critical value of tearing energy increment ΔT_{cr} leading to rupture.

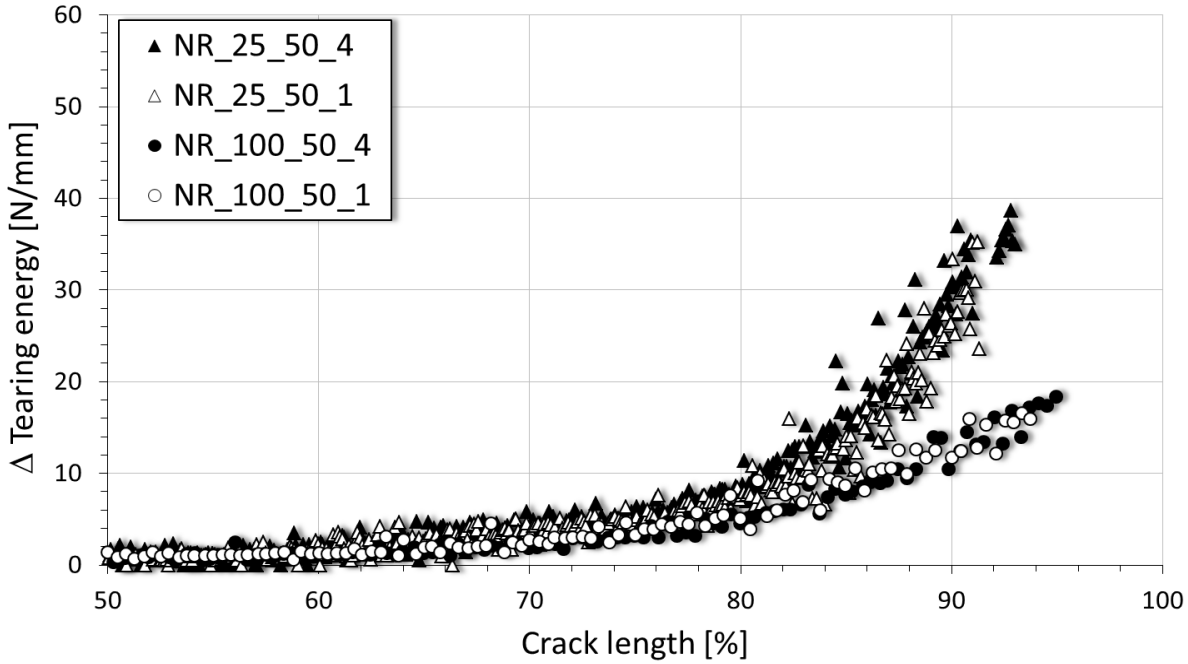

Figure 42. Dependence of tearing energy increment vs. crack length of NR pre-stressed by force 50 N and notched by 0,1 and 0,4 mm thick razor blade with velocity of 25 and 100 mm/min.

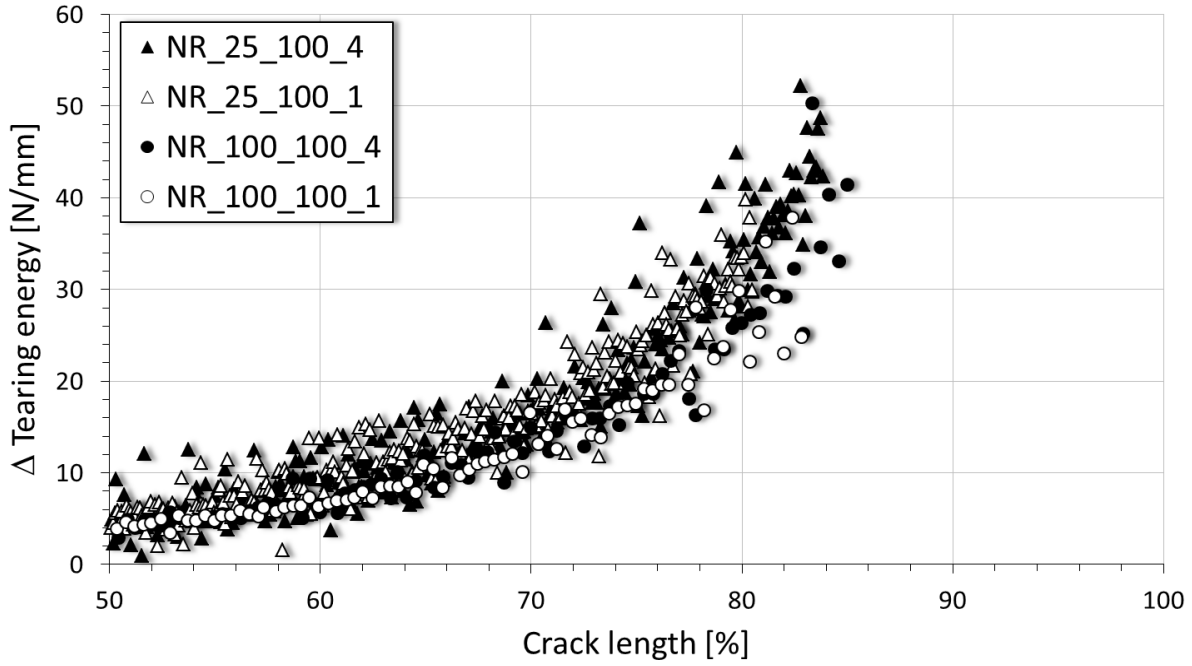

Figure 43. Dependence of tearing energy increment vs. crack length of NR pre-stressed by force 100 N and notched by 0,1 and 0,4 mm thick razor blade with velocity of 25 and 100 mm/min.

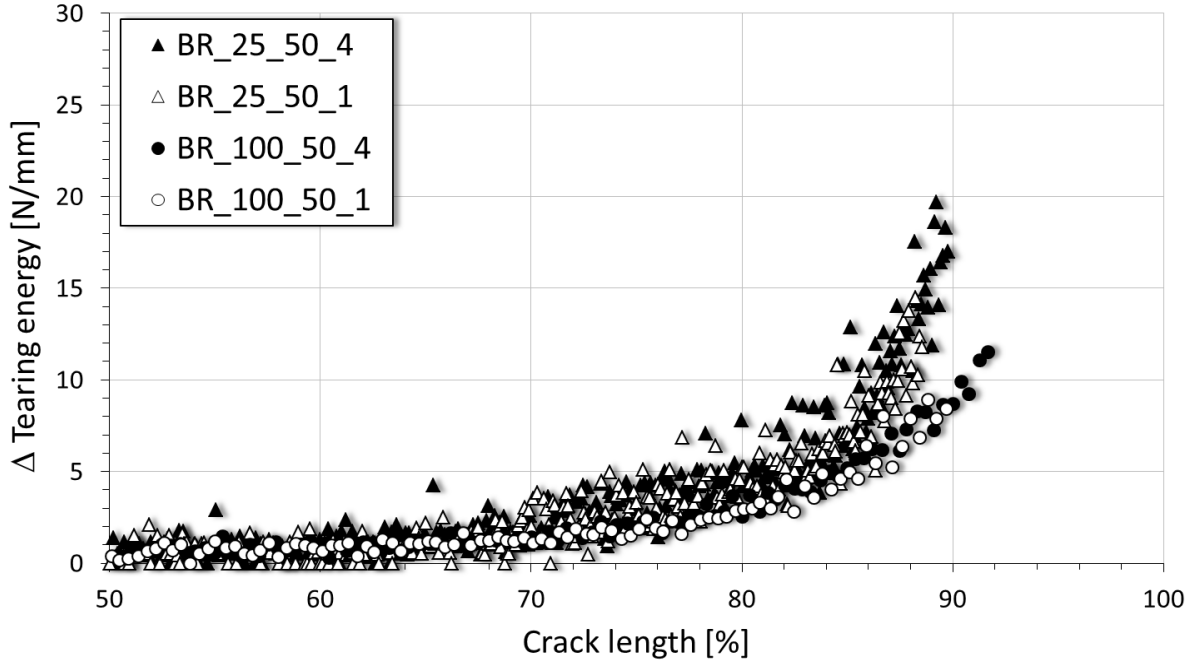

Figure 44. Dependence of tearing energy increment vs. crack length of BR pre-stressed by force 50 N and notched by 0,1 and 0,4 mm thick razor blade with velocity of 25 and 100 mm/min.

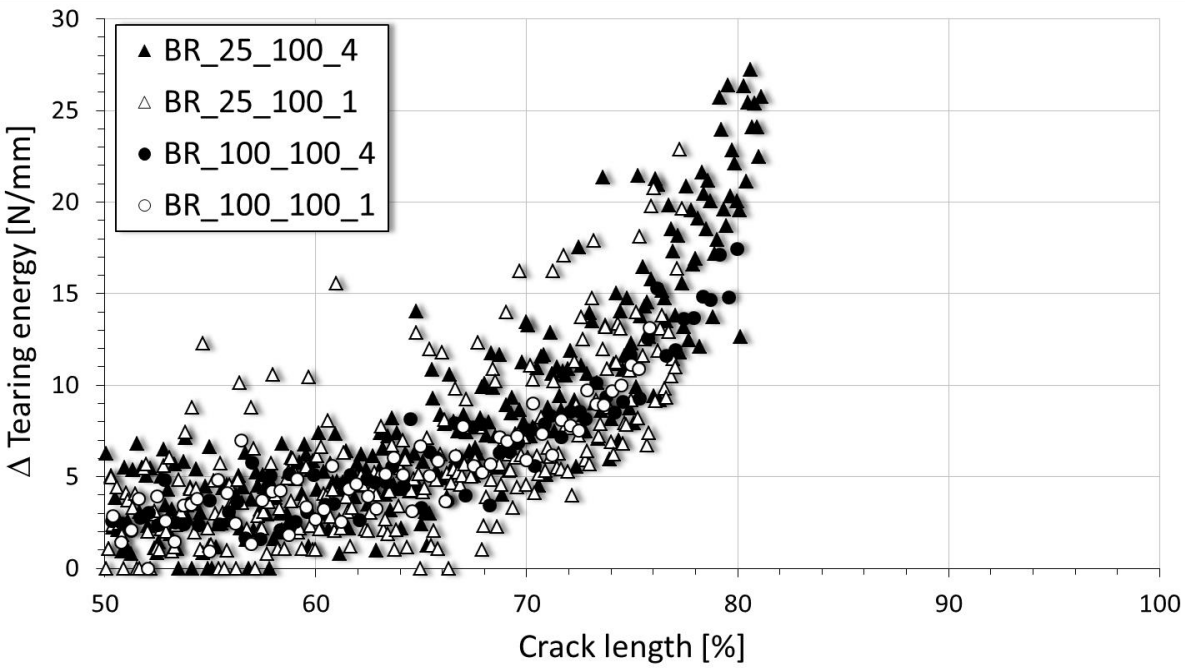

Figure 45. Dependence of tearing energy increment vs. crack length of BR pre-stressed by force 100 N and notched by 0,1 and 0,4 mm thick razor blade with velocity of 25 and 100 mm/min.

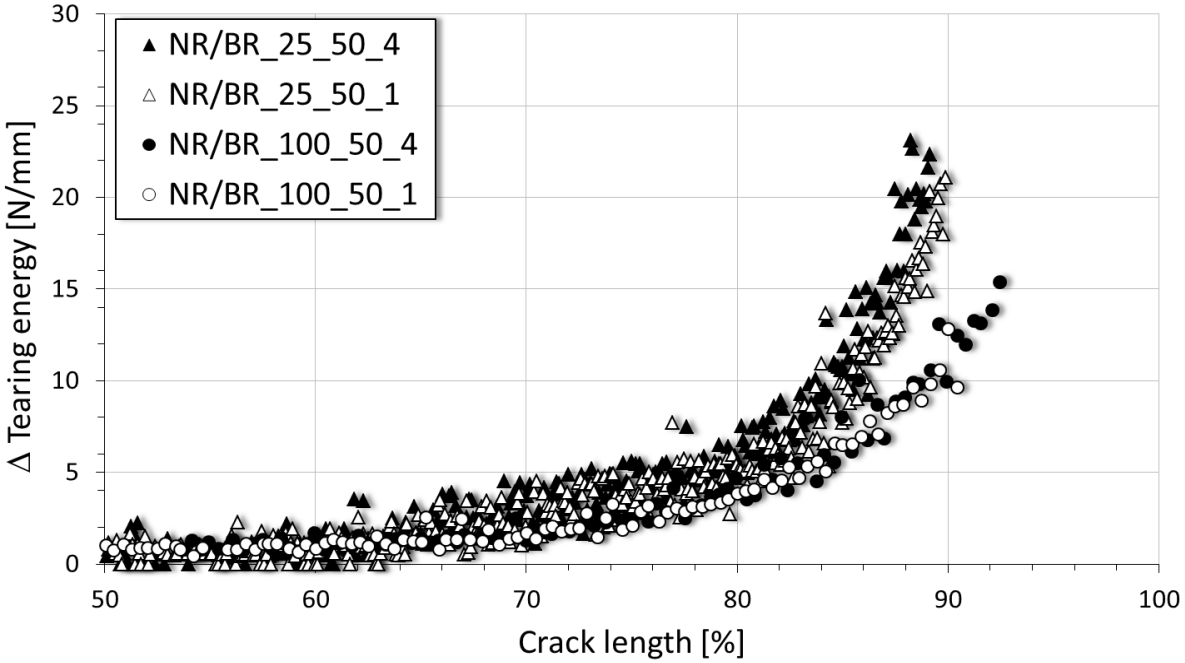

Figure 46. Dependence of tearing energy increment vs. crack length of NR/BR pre-stressed by force 50 N and notched by 0,1 and 0,4 mm thick razor blade with velocity of 25 and 100 mm/min.

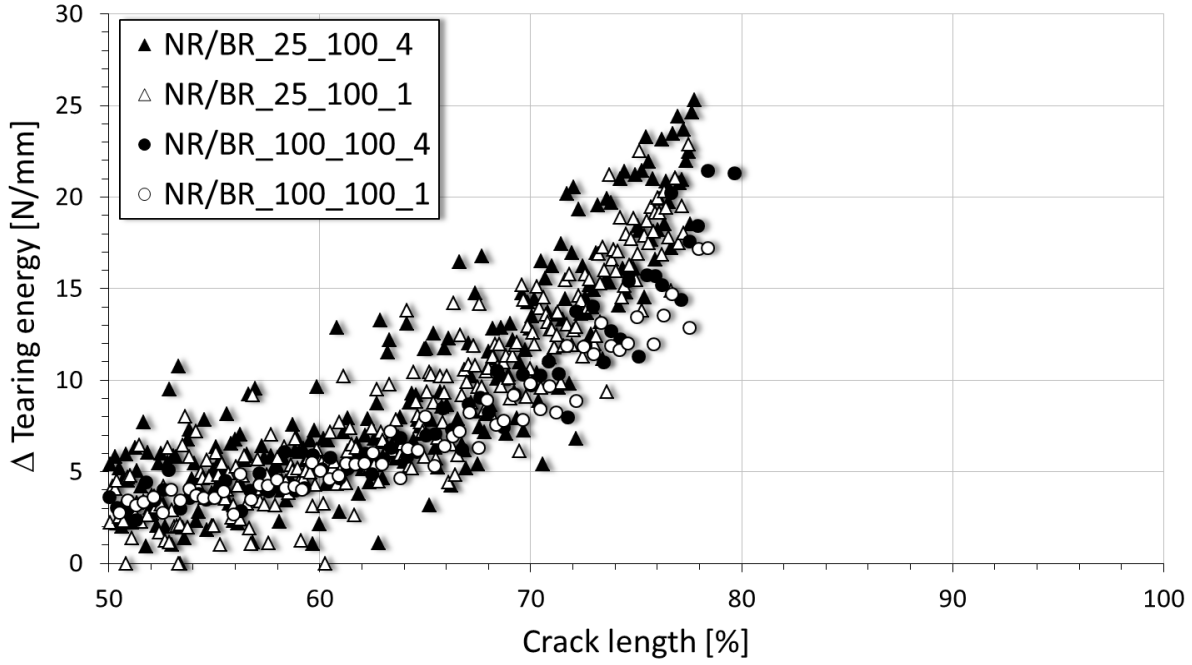

Figure 47. Dependence of tearing energy increment vs. crack length of NR/BR pre-stressed by force 100 N and notched by 0,1 and 0,4 mm thick razor blade with velocity of 25 and 100 mm/min.

From T-a diagrams illustrated in Figures 42 – 47 it is evident that amount of energy necessary to crack propagation goes down with growing content of BR for both loading forces and cutting velocities. Furthermore, it is visible that tearing energy of all tested materials slightly increases approximately at the crack length 50 % and 30 % of the test specimen width for loading 50 N and 100 N, respectively. This is due to higher contribution of strain energy. In addition, the value of critical increment of tearing energy $\Delta\ T_{cr}$ determining the tear strength of rubber, which characterizes unstable crack growth and is dependent on size of loading force and type of tested material, was determined. From results it is obvious, that value of critical tearing energy increment is higher for NR than for NR/BR and BR. Simultaneously, critical length of crack shortens with increasing content of BR in material. Therefore, it is clear that NR vulcanizates exhibit higher crack propagation resistance than BR and their compound for all applied test conditions and thus NR is more durable elastomer. Scattering of tearing energy values of BR loaded by 100 N could be caused by higher crack initiation resistance at higher value of pre-stressed force. Summarizing comparison of results is given by table 4.

Table 4. List of measured fracture characteristics of NR, NR/BR and BR.

	Pre-stressed force, F_y [N]	**50**				**100**			
	Cutting velocity, v_x [mm/min]	**25**	**100**	**25**	**100**	**25**	**100**	**25**	**100**
	Thickness of razor blade. d_b [mm]	**Rupture [%]**		**Critical ΔT [N/mm]**		**Rupture [%]**		**Critical ΔT [N/mm]**	
BR	**0,1**	88,5	89,7	14,5	8,4	77,4	75,8	22,9	13,1
		± 4,6	± 3,8	± 0,9	± 0,5	± 3,5	± 5,1	± 2,1	± 1,2
	0,4	89,8	91,7	19,7	11,6	81,1	80,0	27,2	17,5
		± 3,7	± 5,7	± 1,5	± 0,8	± 4,4	± 6,4	± 2,5	± 2,1
NR/BR	**0,1**	89,9	90,0	21,1	12,8	77,5	78,0	22,9	17,8
		± 3,2	± 4,4	± 1,3	± 1,8	± 6,5	± 4,9	± 0,9	± 2,5
	0,4	89,2	92,5	23,1	15,4	77,8	79,7	25,3	21,3
		± 4,5	± 5,8	± 2,1	± 1,1	± 7,5	± 5,2	± 1,7	± 1,4
NR	**0,1**	91,3	93,7	35,2	15,9	80,5	82,4	39,9	37,8
		± 3,4	± 3,9	± 2,8	± 2,7	± 4,8	± 6,7	± 3,8	± 2,9
	0,4	93,1	95,0	38,7	16,9	83,8	85,0	52,2	41,4
		± 4,9	± 4,8	± 3,4	± 2,1	± 3,7	± 4,1	± 4,1	± 4,9

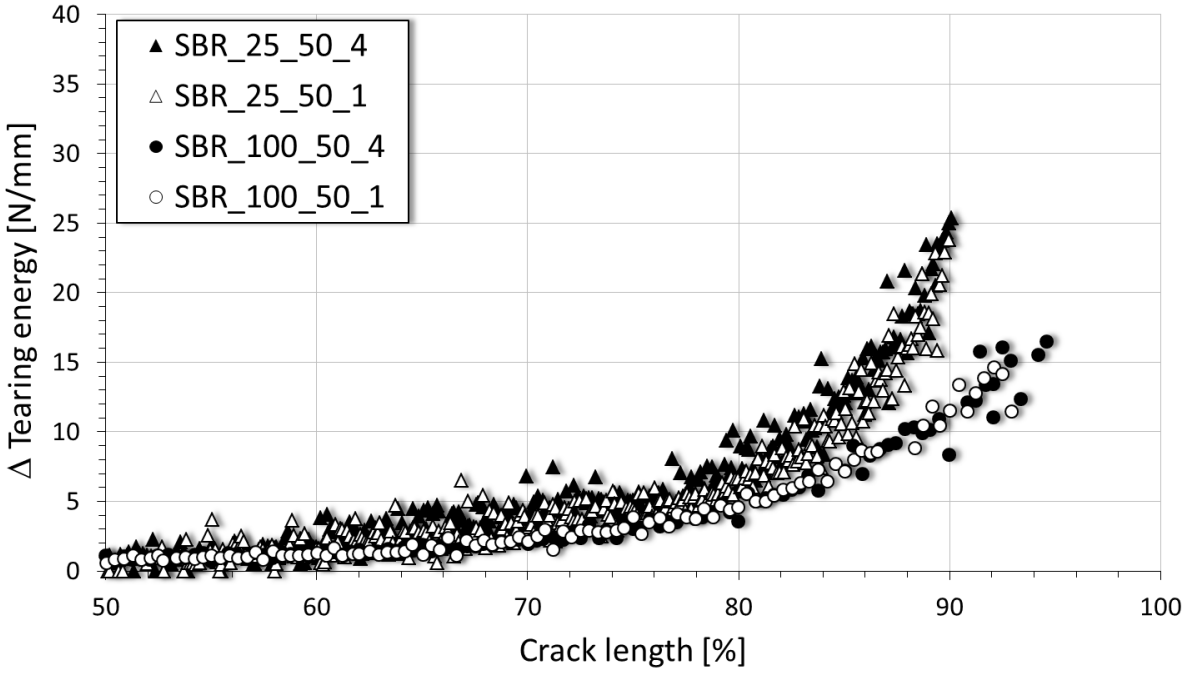

Figure 48. Dependence of tearing energy increment vs. crack length of SBR pre-stressed by force 50 N and notched by 0,1 and 0,4 mm thick razor blade with velocity of 25 and 100 mm/min.

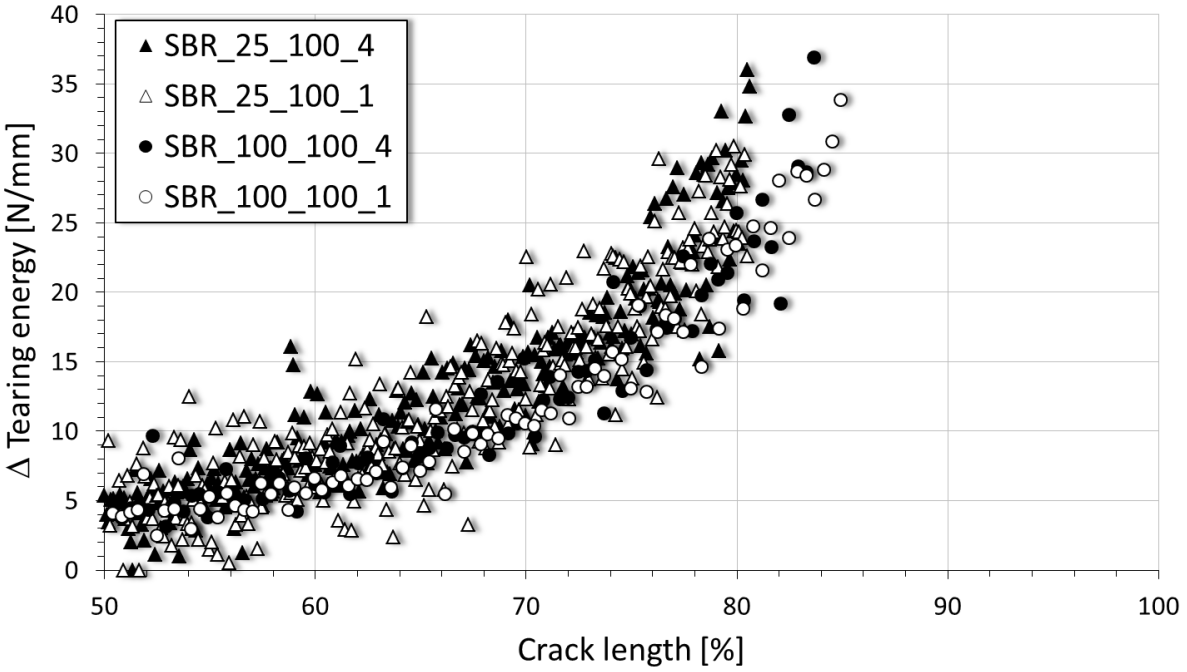

Figure 49. Dependence of tearing energy increment vs. crack length of SBR pre-stressed by force 100 N and notched by 0,1 and 0,4 mm thick razor blade with velocity of 25 and 100 mm/min.

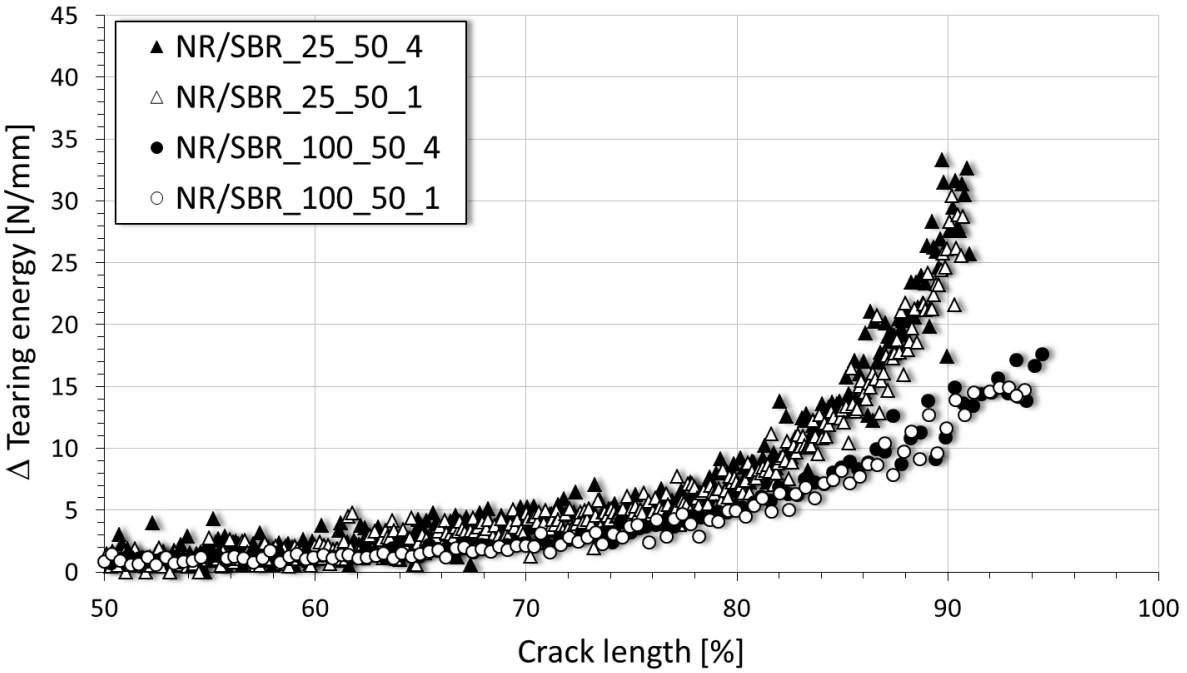

Figure 50. Dependence of tearing energy increment vs. crack length of NR/SBR pre-stressed by force 50 N and notched by 0,1 and 0,4 mm thick razor blade with velocity of 25 and 100 mm/min.

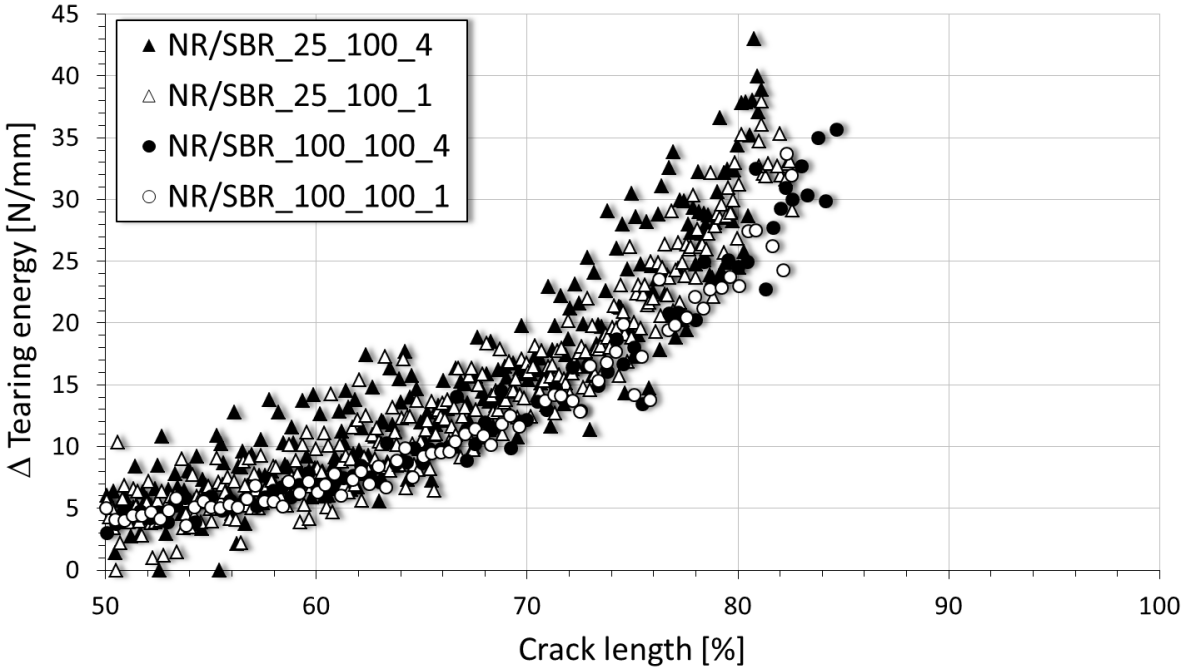

Figure 51. Dependence of tearing energy increment vs. crack length of NR/SBR pre-stressed by force 100 N and notched by 0,1 and 0,4 mm thick razor blade with velocity of 25 and 100 mm/min.

In Figures 48 – 51 there are diagrams displaying progress of tearing energy increment on crack length which provides information about influence of SBR content on fracture behaviour. It is seen that increment of energy necessary to crack propagation as well as its critical value slightly declines with growing content of SBR for both loading forces and cutting velocities, respectively. This decline is not as significant as in case of content of BR. Critical crack length is almost equal for NR and NR/SBR and also SBR. Table 5 shows a summary of results.

Table 5. List of measured fracture characteristics of NR, NR/SBR and SBR.

	Pre-stressed force, F_y [N]	**50**				**100**			
	Cutting velocity, v_x [mm/min]	**25**	**100**	**25**	**100**	**25**	**100**	**25**	**100**
	Thickness of razor blade. *db* [mm]	**Rupture [%]**		**Critical Δ*T* [N/mm]**		**Rupture [%]**		**Critical Δ*T* [N/mm]**	
SBR	**0,1**	90,4	92,1	23,8	14,6	81,1	85,0	30,5	33,9
		± 8,1	± 7,7	± 1,9	± 1,1	± 3,4	± 5,4	± 2,1	± 2,1
	0,4	90,3	94,6	25,3	16,5	81,0	83,7	36,0	36,9
		± 7,2	± 9,2	± 2,0	± 1,4	± 5,4	± 4,2	± 3,8	± 1,7
NR/SBR	**0,1**	90,8	93,9	30,4	15,7	83,1	82,3	38,0	33,7
		± 8,8	± 9,5	± 1,8	± 1,6	± 4,5	± 8,2	± 2,2	± 3,1
	0,4	91,0	95,5	33,3	17,6	81,1	84,7	43,0	35,7
		± 6,3	± 6,2	± 0,9	± 1,8	± 6,8	± 6,7	± 4,8	± 2,7
NR	**0,1**	91,3	93,7	35,2	15,9	80,5	82,4	39,9	37,8
		± 8,4	± 5,9	± 3,1	± 2,3	± 6,6	± 6,1	± 3,3	± 3,7
	0,4	93,1	95,0	38,7	16,9	83,8	85,0	52,2	41,4
		± 8,2	± 7,1	± 2,8	± 1,3	± 7,2	± 7,4	± 3,8	± 3,4

From obtained results, it is visible that BR and its compound with NR exhibit the lowest crack propagation resistance in comparison with NR, SBR and their compounds. Moreover, it is seen that strain energy necessary to crack growth is higher for cutting using thicker razor blade which corresponds with Equation 9. For higher velocity of razor blade movement value of tearing energy is lower due to greater contribution of cutting energy on crack propagation.

4.2.6 Determination of resistance against crack initiation by cutting with sharp object

Characterization of crack initiation resistance was performed using improved version of device measuring stress states in rubber specimen which was cut by a sharp object. This improved version is able to measure applied cutting force and movement of razor blade more accurately and therefore it can be used for crack growth rate characterization at small area. In table 6 conditions which were used for observation of movement velocity of razor blade through the sample to a length of 10 mm are shown. For a purpose to describe differences in crack

growth velocity during cutting process, the distance of 10 mm was divided into five points with 2 mm length. The change of crack growth rate, *da/dt* depends on tearing energy, *T* is represented by double logarithmic plot.

Table 6. List of applied testing conditions used for crack initiation resistance.

Designation	**Cutting force, F_x [N]**	**Pre-force of test specimen, F_y [N]**	**Thickness of razor blade, d_b [mm]**
XX_2_50	2	50	0,1
XX_2_100	2	100	0,1
XX_3_50	3	50	0,1
XX_3_100	3	100	0,1

XX – BR, NR/BR, NR, NR/SBR, SBR

Three standard pure-shear geometry specimens with length to width ratio of 8:1 were analysed for each pre-set condition and average values are plotted as results in following Figures 52-56.

The designation of each test specimen set is given by the code:

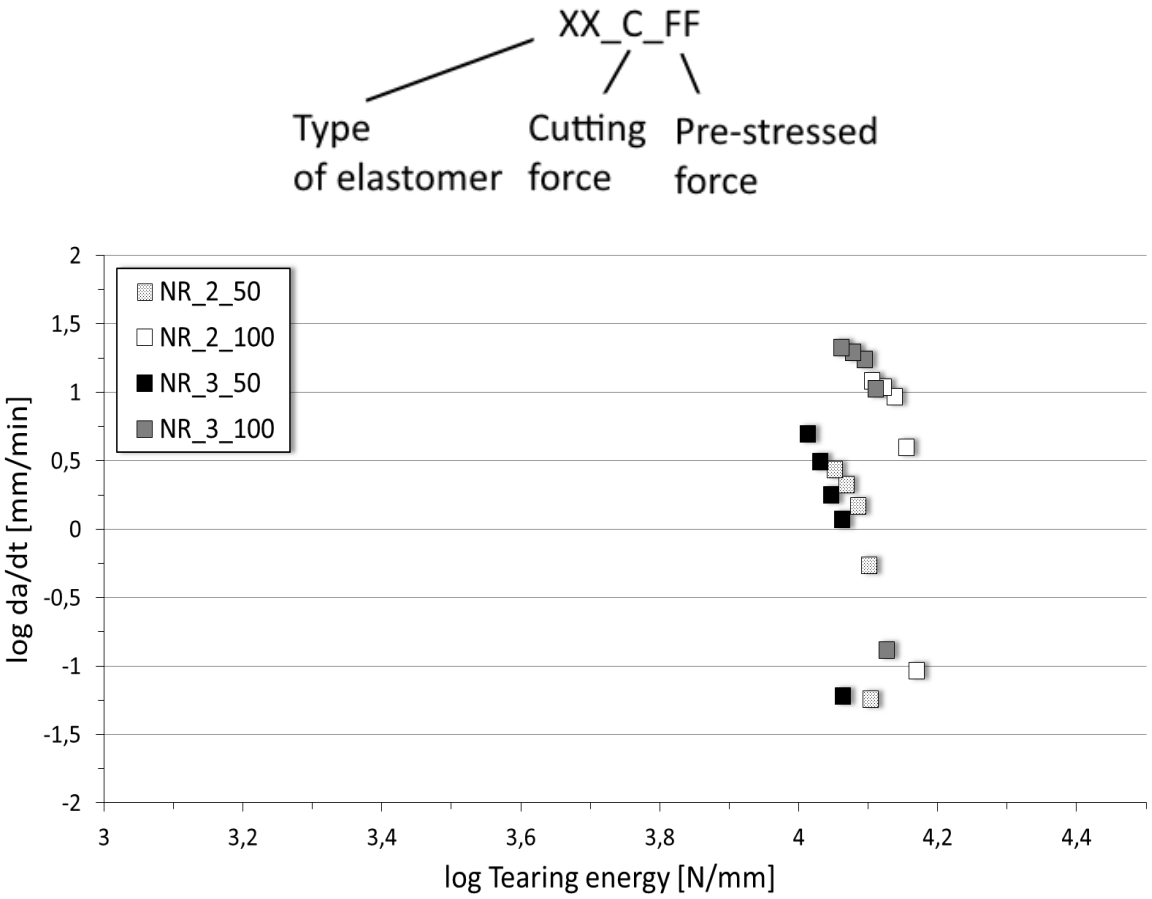

Figure 52. Dependence of crack growth rate vs. tearing energy of NR pre-stressed by force 50 N and 100 N and notched by 0,1 mm thick razor blade by force 2 and 3 N.

From results of NR it is visible that crack growth rate at the first 2 mm of crack length is significantly lower than its values of further points of crack length. It is given by increased initial resistance to cut. Reduction of initial resistance with increasing crack length resulting in decrease of energy required for crack extension of 2 mm, and simultaneously, increase of crack growth rate is detectable. Nevertheless, it is evident, when a specimen is cut by lower force, amount of energy necessary to crack propagation slightly growing.

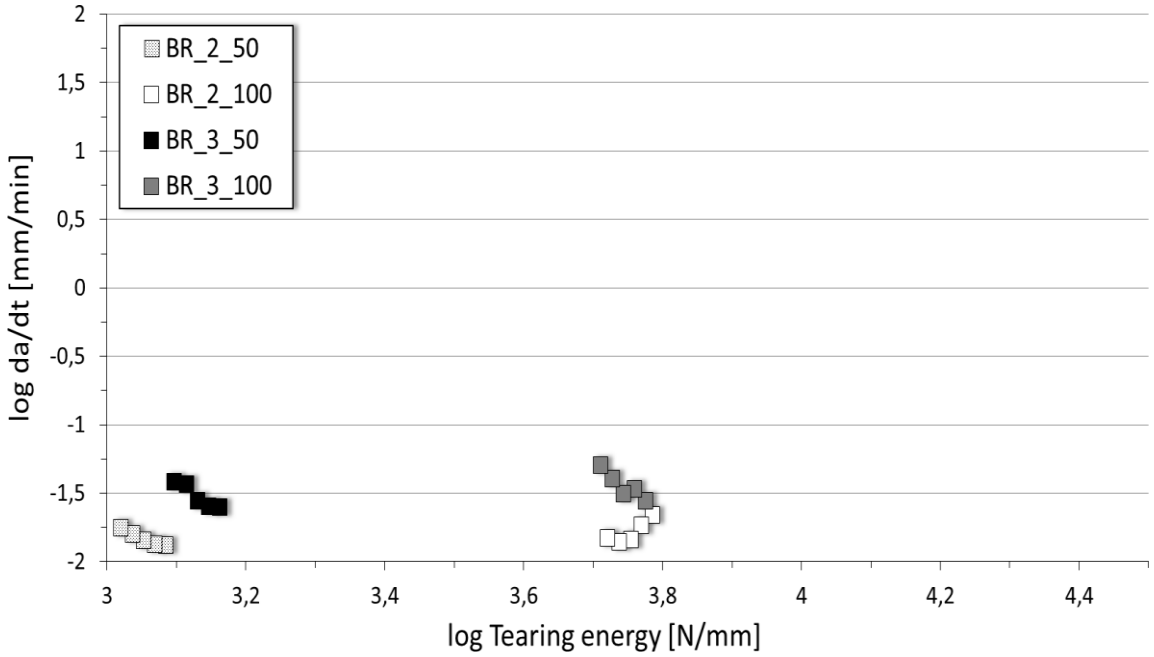

Figure 53. Dependence of crack growth rate vs. tearing energy of BR pre-stressed by force 50 N and 100 N and notched by 0,1 mm thick razor blade by force 2 and 3 N.

In contrast, BR exhibits low crack growth rate indicating good crack initiation resistance compared to the NR. Gradual increase of crack growth rate is visible for all specimens except specimens that were loaded by 100 N and cut by 2 N. Specimens studied at these conditions were characterized by gradual decrease of crack growth rate in dependence on crack length. This phenomenon was observed using different loading forces. In Table 7 progress of crack growth rate of specimens which were loaded by 50, 75 and 100 N is shown.

Table 7. List of measured crack growth velocities of BR pre-stressed by force 50 and 75 N and notched by 0,1 mm thick razor blade by force 2 N.

Crack length [mm]	**Crack growth velocity [mm/min]**		
	BR_2_50	**BR_2_75**	**BR_2_100**
2	0,0132	0,0159	0,0219
4	0,0135	0,0156	0,0185
6	0,0144	0,0316	0,0145
8	0,0160	0,0261	0,0139
10	0,0178	0,0185	0,0149

From results shown in Table 7 it is evident that material based only on BR which is loaded by force higher than 50 N shows ability to reinforce in time, which causes gradual decrease of crack growth rate. This phenomenon could be also confirmed in Figure 45 where is visible the scattering of tearing energy values of BR loaded by higher force. This behaviour may be the result of increase crack propagation resistance at higher value of pre-stressed force.

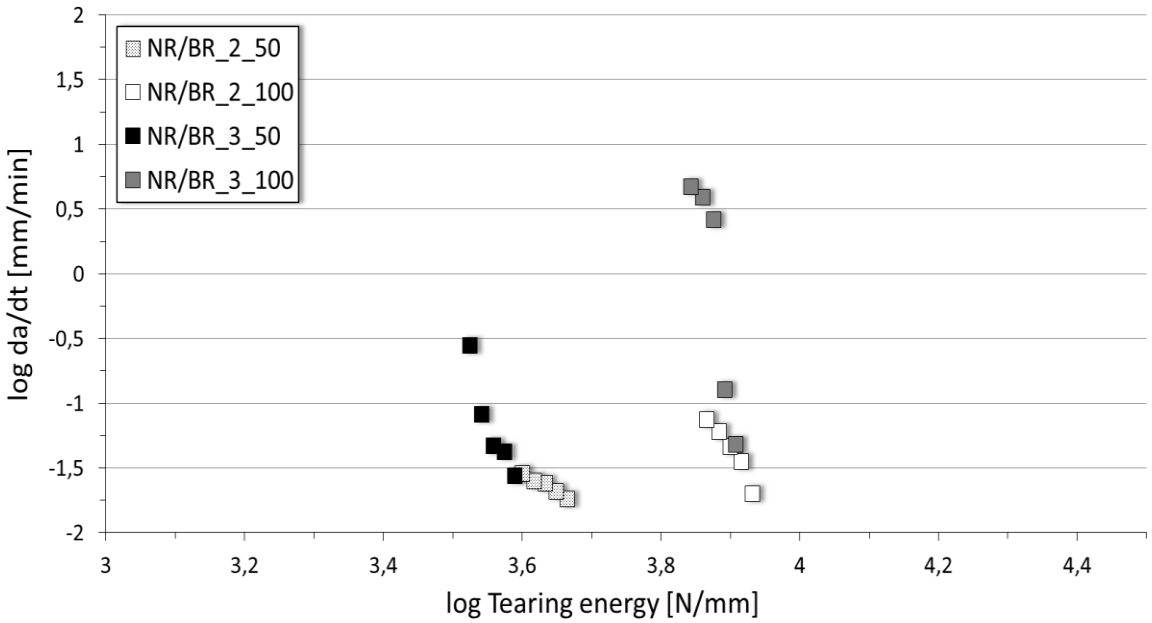

Figure 54. Dependence of crack growth rate vs. tearing energy of NR/BR pre-stressed by force 50 N and 100 N and notched by 0,1 mm thick razor blade by force 2 and 3 N.

Compound consisting NR and BR is represented by fracture behaviour influenced by contribution both elastomers. NR in compound improves crack growth resistance. That is demonstrated by increasing amount of energy necessary to crack growth. On the other hand, there is visible decline of crack growth rate in comparison with NR that is noticeable influence of BR.

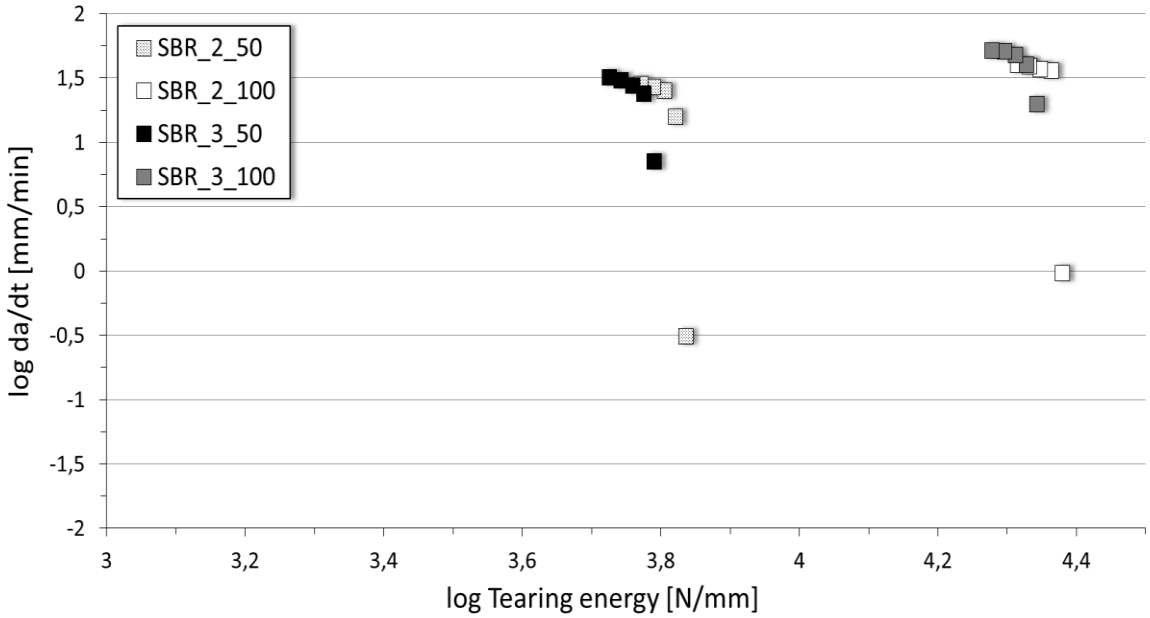

Figure 55. Dependence of crack growth rate vs. tearing energy of SBR pre-stressed by force 50 N and 100 N and notched by 0,1 mm thick razor blade by force 2 and 3 N.

According to the results published in Figure 55 it is visible, that SBR exhibits the highest values of crack growth rate. It is a feature of low resistance to propagation of crack formed by sharp object. Energy necessary to crack propagation is slightly higher than for NR except specimens loaded by force of 50 N. Resistance to crack initiation and propagation is low, therefore there is not enough time for creep process leading to bigger amount of energy absorption than in case of NR.

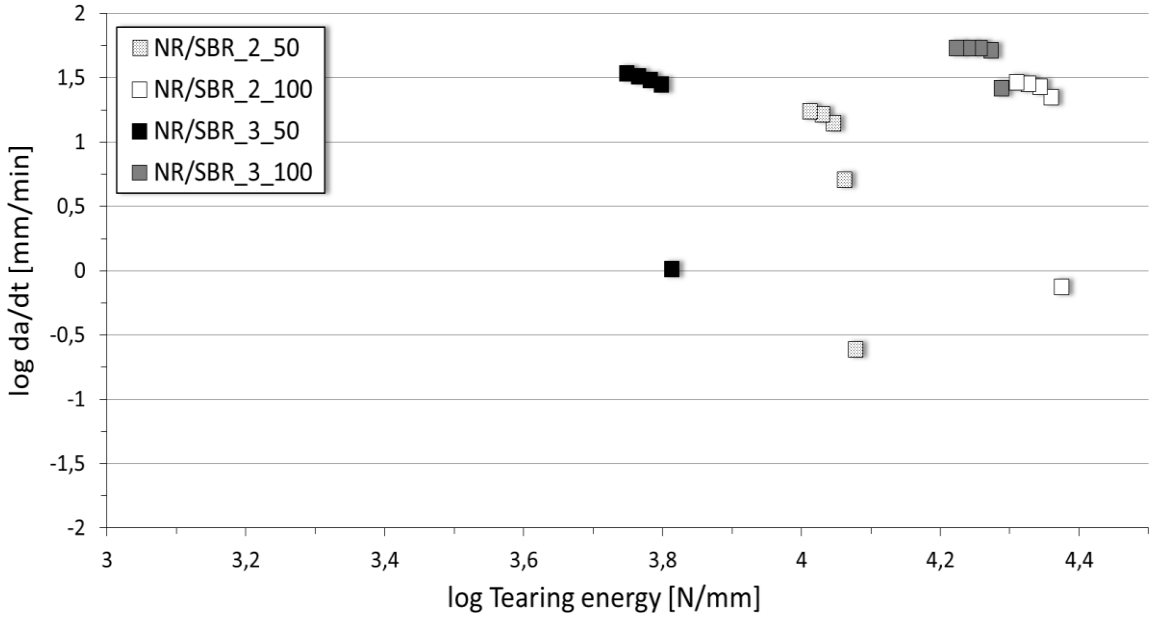

Figure 56. Dependence of crack growth rate vs. tearing energy of NR/SBR pre-stressed by force 50 N and 100 N and notched by 0,1 mm thick razor blade by force 2 and 3 N.

In Figure 56 results of material which was formed by NR and SBR can be seen. This material has approximately the same values of crack growth rate like SBR. However, effect of NR content is visible for specimens which were loaded by 50 N where NR evidently improves crack initiation resistance. Values of crack growth rate are lower than for SBR and moreover energy necessary to crack growth achieves higher values.

5. CONCLUSION

Presented thesis was conducted to make a theoretical summary focused on fracture mechanics of rubber. The theoretical background was supplemented with experimental part containing a collection of basic mechanical testing methods usable for characterization of mechanical and fracture behaviour of rubber. Rubber compounds based on NR, BR, and SBR filled by carbon black were used as standard materials for investigation of fracture behaviour.

A few mechanical testing methods working quasi-statically and cyclically were performed in order to describe fracture behaviour at different shape of loading waveform. The initial process leading to failure of rubber product is represented by formation of crack being able to propagate when value of supplied energy is high enough. In this work, methods describing crack initiation resistance at low and high velocities were performed.

Conventional abrasion test was used to determine crack initiation resistance of rubber at low velocities. It is evident that BR increases resistance against crack initiation whereas SBR has the opposite effect.

In contrast, free falling dart method was used to characterize durability of rubber specimens without any macro cracks at high speed. The first phase of specimen penetration describes resistance to crack formation. From these results it is visible, that addition of BR also leads to improve crack initiation resistance at high velocities, and however material prepared only from SBR exhibits the highest energy necessary to crack formation. Furthermore, the data obtained by free falling dart test could be used to determine amount of energy necessary to break specimen, thus propagation of crack. Data analysis has shown that growing concentration of BR leads to increase of resilience.

When the energy supplied in specimen with presence of flaws and macro cracks is sufficiently large, crack propagation occurs. Rubber resistance to crack propagation was measured in impact and cyclically in tension using notched specimen. The impact tensile test was used to evaluate crack propagation resistance at high velocities, especially the effect on ratio between stable and unstable crack growth region. Moreover, influence of temperature was investigated. It is visible from the obtained results, that BR exhibits low resistance to crack propagation at both regions. However, the resistance increases with decreasing temperature. SBR exhibits an improvement of crack propagation resistance in comparison with NR. But this property is noticeable only for temperatures higher than temperature of glass transition which is given by peak of Tan delta. Furthermore, influence of elastomer type on rate of ability to absorb strain energy without failure was characterized. It is shown that BR exhibits the lowest level of impact toughness from tested materials and the property is positively influenced by decreasing temperature. On the contrary SBR has positive effect on impact toughness.

In case of fatigue crack propagation resistance, sinusoidal cyclic loading in tension was carried out. From dependence of tearing energy on crack growth rate it is visible that NR achieves the lowest level of crack growth rate which is a sign of good crack propagation resistance whereas the worst resistance is detected for BR.

In addition, as part of published research a new device to investigate stress states into specimen which is loaded in tension and simultaneously cut by sharp object has been introduced. Resistance to crack initiation and propagation was described using this device. From obtained data it is confirmed that BR exhibits the best resistance to crack initiation in comparison with NR and SBR which exhibits the worst resistance. In the case of propagation, the best properties were described for NR whereas BR has the lowest durability. In addition, it was confirmed that the energy necessary to crack propagation decreases with decreasing radius of crack tip.

In conclusion, the experimental work summarizes various common testing methods and demonstrates the ability of the simple methodology to characterize the complex fracture properties of rubber materials to predict the final rubber product behaviour. It was found out that published testing methods are useable for description of processes leading to mechanical failure of rubber as well as for fracture properties description of tested rubber compounds. Further, the device able to characterize resistance against penetration of sharp object into pre-stressed rubber test specimen was introduced. Using this device, good crack initiation resistance of BR and good durability of NR was confirmed. Thus it could be said that the newly developed device can be used for characterization of crack initiation resistance and is able to fully substitute the abrasive test device. Moreover, the crack propagation resistance can be promptly measured using this device.

References

[1] Sommer JG. *Engineered Rubber Products - Introduction to Design, Manufacture and Testing*. Hanser Publishers, 2009. Electronic ISBN 978-1-61344-301-9.

[2] Hertz DL. *Introduction*. In: Gent AN. *Engineering with Rubber - How to Design Rubber Components*. 3rd ed.: Hanser Publishers, 2012, 2-9. Electronic ISBN 978-1-61344-659-1.

[3] Erman B, Mark JE, Roland MC. *Science and Technology of Rubber*. 4th ed.: Elsevier, 2013. Electronic ISBN: 978-0-12-394832-8.

[4] Tomsic JL. *Dictionary of Materials and Testing*. 2nd ed.: SAE International, 2000. Electronic ISBN: 978-1-61583-648-2.

[5] Guo Z, Sluys LJ. *Constitutive modelling of hyperelastic rubber-like materials*. HERON, 2008; 53 (3), 109-132.

[6] Dick JS. *Basic Rubber Testing - Selecting Methods for A Rubber Test Program*. ASTM International, 2003. Electronic ISBN: 978-1-60119-436-7.

[7] Mars WV, Fatemi A. A literature survey on fatigue analysis approaches for rubber. *International Journal of Fatigue*, 2002; 24, 949-961. ISSN: 0142-1123.

[8] Ellul MD. *Mechanical Fatigue*. In: Gent AN. *Engineering with Rubber - How to Design Rubber Components*. 3rd ed.: Hanser Publishers, 2012, 139-176. Electronic ISBN 978-1-61344-659-1.

[9] Lake GJ, Lindley PB. The Mechanical Fatigue Limit for Rubber. *Journal of Applied Polymer Science*, 1965; 9, 1233-1251.

[10] Macdonald KA. *Fracture and Fatigue of Welded Joints and Structures*. Woodhead Publishing, 2011. Electronic ISBN: 978-0-85-709250-2.

[11] South JT. Mechanical Properties and Durability of Natural Rubber Compounds and Composites. Faculty of the Virginia Polytechnic Institute and State University, Materials Engineering Science, 2001, PhD. Thesis.

[12] Gengsheng W. et al. Crack Initiation and Evolution in Vulcanized Natural Rubber Under High Temperature Fatigue. *Polymer Degradation and Stability*, 2011; 96 (12), 2221-2228.

[13] Cadwell SM. et al. Dynamic Fatigue Life of Rubber. *Rubber Chemistry and Technology*, 1940; 13, 304-315.

[14] Beatty JR. Fatigue of Rubber. *Rubber Chemistry and Technology*, 1964; 37, 1341-1364.

[15] Gent AN, Lindley PB, Thomas AG. Cut growth and fatigue of rubbers. I. The relationship between cut growth and fatigue. *Journal of Applied Polymer Science*, 1964; 8, 455-466.

[16] Lee MP, Moet A. Analysis of Fatigue Crack Propagation in NR/BR Rubber Blend. *Rubber Chemistry and Technology*, 1993; 66, 304-316.

[17] Griffith AA. The Theory of Rupture. 1st International Congress on Applied Mechanics : s.n., 1925. pp. 55-63.

[18] Kanninen MF, Popelar CH. *Advanced Fracture Mechanics*.: Oxford University Press, 1985. Electronic ISBN: 978-1-61583-231-6.

[19] Wei RP. *Fracture Mechanics - Integration of Mechanics, Materials Science, and Chemistry*.: Cambridge University Press, 2010. Electronic ISBN: 978-0-511-68471-5.

[20] Roylance D. *Introduction to Fracture Mechanics*. Massachusetts Institute of Technology, 2001.

[21] Milne I, Ritchie RO, Karihaloo B. *Comprehensive Structural Integrity, Volumes 1-10*. Elsevier, 2003. Electronic ISBN: 978-0-08-049073-1.

[22] Wiesner CS. *Crack Arrest Concepts for Failure Prevention and Life Extension*. Woodhead Publishing, 1996. ISBN: 9781855732643.

[23] Irwin GR. Crack-Extension Force for a Part-Through Crack in a Plate. *Journal of Applied Mechanics*, 1962; 29 (4), 651-654.

[24] Anderson RB, Holms AG, Orange TW. *Stress Intensity Magnification for Deep surface Cracks in Sheets and Plates*. Washington, D.C. : National Aeronautics and Space Administration, 1970.

[25] Rice JR. A Path Independent Integral and the Approximate Analysis of Strain Concentration by Notches and Cracks. *Journal of Applied Mechanics*, 1968; 35, 379-386.

[26] Vukelić G, Brnić J. J-integral as Possible Criterion in Material Fracture Toughness Assessment. *Engineering Review*, 2011; 31 (2), 91-96.

[27] Lee DJ, Donovan JA. Critical J-Integral and Tearing Energies for Fracture of Reinforced Natural Rubber. *Theoretical and Applied Fracture Mechanics*, 1985; 4, 137-147.

[28] Amar MB, Rice JR. Exact results with the J-integral applied to free-boundary flows. *Journal of Fluid Mechanics*, 2002; 461, 321-341.

[29] Gent AN, Schultz J. Effect of wetting liquids on strength of adhesion of viscoelastic materials. *Journal Adhesion*, 1972; 3, 281-294.

[30] Guillement J, Bistac S, Schultz J. Relationship between polymer viscoelastic properties and adhesive behaviour. *International Journal of Adhesion and Adhesives*, 22, 2002, 1-5.

[31] Persson BNJ, et al. Crack propagation in rubber-like materials. *Journal of Physics: Condensed Matter*, 2005; 17, 1071-1142

[32] Williams ML, Landel RF, Ferry JD. The temperature dependence of relaxation mechanics in amorphous polymers and other glass forming liquids. *Journal of the American Chemical Society*, 1955, 77, 3701-3707.

[33] Sabu T, et al. *Natural Rubber Materials, Volume 2 - Composites and Nanocomposites*. Royal Society of Chemistry, 2014. Electronic ISBN: 978-1-62870-876-9.

[34] Lake GJ, Lindley PB, Thomas AG. Fracture Mechanics of Rubber.

[35] Gdoutos EE, Daniel IM, Schubel P. Fracture Mechanics of Rubber. Facta Universitas: Mechanics, *Automatic Control and Robotics*, 2003; 3 (13), 497-510.

[36] Stoček R, et al. *Analysis of Dynamic Crack Propagation in Elastomers by Simultaneous Tensile- and Pure-Shear-Mode Testing*. In Grellmann W, et al. *Fracture Mechanics of Reinforced Elastomeric Blends*. Berlin : Springer, 2013. ISSN 1613-7736.

[37] Thomas AG. The Development of Fracture Mechanics for Elastomers. *Rubber Chemistry and Technology*, 1994; 67, G50-G60.

[38] Bauman JT. *Fatigue, Stress, and Strain of Rubber Components - A Guide for Design Engineers*. Hanser Publishers, 2008. Electronic ISBN: 978-1-61344-292-0.

[39] Grellmann W, Reincke K. *Technical Material Diagnostics - Fracture Mechanics of Filled Elastomer Blends*. In Grellmann W, et al. *Fracture Mechanics of Reinforced Elastomeric Blends*. Berlin : Springer, 2013. ISSN 1613-7736.

[40] Sakulkaew K, Thomas AG, Busfield JJC. The Effect of The Rate of Strain on Tearing in Rubber. *Polymer Testing*, 2011; 30, 163-172.

[41] *Dictionary of Metals*. ASTM International, 2012. Electronic ISBN: 978-1-62198-375-0.

[42] Mars WV, Fatemi A. Factors That Effect The Fatigue Life of Rubber: A Literature Survey. *Journal of Rubber Chemistry and Technology*, 2004; 77 (3), 391-412.

[43] Thomas AG. Rupture of Rubber. V. Cut Growth in Natural Rubber Vulcanizates. *Journal of Polymer Science*, 1958; 31, 467-480.

[44] Lake GJ. Aspects of Fatigue and Fracture of Rubber. *Progress of Rubber Technology*, 1983; 45, 89-143.

[45] Lindley PB. Non-relaxing Crack Growth and Fatigue in a Noncrystallizing Rubber. *Rubber Chemistry and Technology*, 1974; 47, 1253-1264.

[46] Ghosh P, Mukhopadhyay R, Kankroli, Rajasthan, Stoček R. Durability Prediction of NR/BR and NR/SBR Blend Tread Compounds Using Tear Fatigue Analyser. *Kautschuk Gummi Kunststoffe* - in press.

[47] Hardy D, et al. Paper No. 2 presented at RubberChem'99 Belgium. 1999.

[48] Ghosh P, et al. ECCMR. Paris : s.n., 2007. Viscoelastic material property characterization for tyre finite element analysis. pp. 317-323.

[49] Ghosh P, Stoček R, Gehde M, Mukhopadhyay K, Krishnakumar R. Investigation of fatigue crack growth characteristics of NR/BR blend based tyre tread compounds. *International Journal of Fracture*, 2014; 188 (1), 9-21. ISSN: 0376-9429

[50] Lake GJ, Thomas AG, Roberts AD. Strength properties of Rubber. *Natural Rubber Science and Technology*. Oxford University Press. 1988, 731-772.

[51] Lake GJ, et al. Kuala Lumpur : International Rubber Conference, 1975.

[52] Mullins L. Rupture of Rubber. IX. Role of Hysteresis in the Tearing of Rubber. *Transactions of the Institution of the Rubber Industry*, 1959; 35, 213-222.

[53] Ahagon A, Gent AN, Kim HJ, Kumagai Y. Fracture energy of elastomers in mode I (cleavage) and mode III (lateral shear). *Rubber Chemistry and Technology*. 1975, 48,896 -901.

[54] Andrews EH. Crack Propagation in Strain-crystallizing Elastomer. *Journal of Applied Physics*, 1961; 32, 542-548.

[55] Lake GJ, Lindley PB. Cut Growth and Fatigue of Rubbers. II. Experiments on a Noncrystallizing Rubber. *Journal of Applied Polymer Science*, 1964; 8, 455-466.

[56] Roland CM. Network Recovery from Uniaxial Extension. I. Elastic Equilibrium. *Rubber Chemistry and Technology*, 1989; 62, 863-879.

[57] Sung-Seen CH, et al. Thermal Aging Behaviors of Elemental Sulfur-Free Polyisoprene Vulcanizates. *Bulletin Korean Chemical Society*, 2005; 26 (11), 1853-1855.

[58] Lyubchanskaya LI, Kuzminskiĭ AS. The Degradation of Main Chains and Crosslinks in the Aging of Vulcanizates. *Rubber Chemistry and Technology*, 1961; 34, 922-924.

[59] Akiba M, Hashim AS. Vulcanisation and crosslinking in elastomers. *Progress in Polymer Science*; 3 (22), 475-521.

[60] Lake JG, Thomas AG. *Strenght*. In: Gent AN. *Engineering with Rubber - How to Design Rubber Components*. 3rd ed.: Hanser Publishers, 2012, 100-135. Electronic ISBN 978-1-61344-659-1.

[61] Stoček, R.; Kratina, O.; Kipscholl, R.:Advanced Industrial Methods for Characterization of Tire Failure, PLASTKO 2014, 8. ─ 9. 4. 2014, ISBN 978-80-7454-335-7.

[62] ISO 8256 (2004): Plastics – Determination of Tensile-Impact Strength.

[63] Grellmann W, Reincke K. *Procedure for Determining the Crack Resistance Behaviour Using the Instrumented Tensile-Impact Test*.[Online]. [viewed 2016-02-03]. Available from: http://www.polymerservice-merseburg.de/fileadmin/sachverstaendigenbuero/pdfs/mpk3_engl.pdf.

[64] Lake GJ, Yeoh, OH. Measurement of rubber cutting resistance in the absence of friction, *International Journal of Fracture*, 1978, 14(5), 509-526.

[65] Stoček R, Kratina O, Euchler E, Kipscholl R. Advanced Methods for Experimental Characterization of Rubber Failure With Respect to Real Loading Condition of Rubber Products in the Field. *Proceeding of 4th International Conference On Fracture Fatigue and Wear*, 293-303. ISSN 2294-7869.

List of symbols and acronyms

α	extension ration
σ	stress in tension
a	crack length
aT	multiplying factor
A	area of one fracture surface
ASTM	American Society for Testing and Materials
b	width of legs
BIIR	bromobutyl rubber
BR	butadiene rubber
CCD	charge-coupled device
CR	polychloroprene rubber
d	thickness of specimen
d_b	thickness of razor blade
DMA	dynamic mechanical analysis
d_n	diameter of notch tip
E	elastic modulus
DENT	double-edge-notched tension
E_{cr}	cracking energy
EPDM	ethylene-propylene rubber
F_I	function of the ratio of the crack length and
FCG	fatigue crack growth
F_{cr}	cracking force
F_{pen}	penetration force
F_x	cutting force
F_y	pre-stressed force
G	crack driving force
HAF	high abrasion furnace carbon black
IIR	butyl rubber
IR	isoprene rubber
ISO	lnternational Organization for Standardization
J	impact toughness
K	stress intensity factor
K_I	stress intensity factor in tension
l	length of specimen
L_o	undeformed height of specimen
MDR	moving die rheometer
MT	medium thermal carbon black
NBR	acrylonitrile-butadiene rubber
NR	natural rubber
P	applied forceR crack grow resistance
SBR	styrene butadiene rubber

SENT	single edge notched tension
t	time
T	tearing energy
T_0	threshold tear energy
T_{cr}	critical tearing energy
T_g	glass transition temperature
TFA	Tear and Fatigue Analyzer
U	elastic energy of the system
U_0	elastic energy of the system without crack
U_a	strain energy
U_γ	surface energy
v_x	cutting velocity
w	strain elastic energy density
W	mechanical work
W_b	work required to break

List of figures

List of tables